

Selective darkening of degenerate transitions for implementing quantum controlled-NOT gates

This article has been downloaded from IOPscience. Please scroll down to see the full text article.

2012 New J. Phys. 14 073038

(<http://iopscience.iop.org/1367-2630/14/7/073038>)

View [the table of contents for this issue](#), or go to the [journal homepage](#) for more

Download details:

IP Address: 134.160.214.34

The article was downloaded on 30/07/2012 at 10:16

Please note that [terms and conditions apply](#).

Selective darkening of degenerate transitions for implementing quantum controlled-NOT gates

P C de Groot^{1,2,6}, S Ashhab^{3,4}, A Lupaşcu⁵, L DiCarlo¹,
Franco Nori^{3,4}, C J P M Harmans¹ and J E Mooij¹

¹ Kavli Institute of Nanoscience, Delft University of Technology, PO Box 5046, 2600 GA Delft, The Netherlands

² Max Planck Institute for Quantum Optics, Garching 85748, Munich, Germany

³ Advanced Science Institute, RIKEN, Wako-shi, Saitama 351-0198, Japan

⁴ Department of Physics, University of Michigan, Ann Arbor, MI 48109-1040, USA

⁵ Institute for Quantum Computing, Waterloo Institute for Nanotechnology, and Department of Physics and Astronomy, University of Waterloo, Waterloo, N2L 5G7, Canada

E-mail: pieter.degroot@lmu.de

New Journal of Physics **14** (2012) 073038 (33pp)

Received 4 February 2012

Published 17 July 2012

Online at <http://www.njp.org/>

doi:10.1088/1367-2630/14/7/073038

Abstract. We present a theoretical analysis of the selective darkening method for implementing quantum controlled-NOT (CNOT) gates. This method, which we have recently proposed and demonstrated, consists of driving two transversely coupled quantum bits (qubits) with a driving field that is resonant with one of the two qubits. For specific relative amplitudes and phases of the driving field felt by the two qubits, one of the two transitions in the degenerate pair is darkened or, in other words, becomes forbidden by effective selection rules. In these driving conditions, the evolution of the two-qubit state realizes a CNOT gate. The gate speed is found to be limited only by the coupling energy J , which is the fundamental speed limit for any entangling gate. Numerical simulations show that at gate speeds corresponding to $0.48J$ and $0.07J$, the gate fidelity is 99% and 99.99%, respectively, and increases further for lower gate speeds. In addition, the effect of higher-lying energy levels and weak anharmonicity is studied, as well as the scalability of the method to systems of multiple qubits. We conclude that in all these respects this method is competitive with existing schemes for creating entanglement, with the added advantages

⁶ Author to whom any correspondence should be addressed.

of being applicable for qubits operating at fixed frequencies (either by design or for the exploitation of coherence sweet-spots) and having the simplicity of microwave-only operation.

Contents

1. Introduction	2
2. Selective darkening	3
2.1. Basic principle	3
2.2. Strong coupling	7
3. Relation to other gates	8
4. Time-domain evolution of the gate and spurious driving of other transitions	9
4.1. Ideal gate evolution under rotating wave approximation	10
4.2. Single- and two-qubit errors caused by the ac-Stark effect	11
5. Numerical simulation of gate dynamics for two-level qubits	12
6. Weakly anharmonic qubits	15
7. Scalability	19
8. Conclusion and discussion	25
Acknowledgments	26
Appendix A. Transformation to rotating frame	26
Appendix B. Quantum mechanical description of the driving field	28
References	31

1. Introduction

An important step towards the realization of a quantum computer is to implement a set of universal gates from which all other operations can be composed. The quantum controlled-NOT (CNOT) gate is a prominent example of a two-qubit universal gate, requiring only the addition of single-qubit gates to form a complete universal set. The physical implementation of a gate depends on the type of qubit that is used, but even for a specific qubit type a certain gate can often be implemented using a variety of methods. The ideal method delivers a gate that is fast compared to qubit decoherence times, has a high fidelity, is simple to implement and does not introduce constraints that compromise the coherence time of the qubits or the implementation of other gates.

One classification of two-qubit gates is based on the required nature of the interaction between the qubits [1]. When the interaction term contains diagonal elements in the single-qubit energy eigenbasis, often referred to as longitudinal or zz -coupling, the transition frequency of one qubit depends on the state of the other qubit. Although this spectroscopic shift enables simple resonant driving for all operations [2, 3], the shift also leads to continuously evolving phases that must be compensated for by refocusing schemes [4]. In contrast, for transverse coupling the energy splitting of one qubit does not depend on the state of the other qubit. In this respect, the system can be described as a set of effectively uncoupled qubits [5, 6]. The desired entangling evolution can then be induced by dynamic manipulation of the system. Clearly, the degeneracy due to the lack of a spectroscopic splitting forbids any method based on frequency

selectivity. Focusing on superconducting qubits [7–15], previous methods used either additional coupling elements [16–29], extra qubit states outside the computational basis [25, 30–32] or shifting levels in and out of resonance by dc [33–35] or strong ac fields [5, 36–38].

Another important consideration is that a method can require certain bias conditions of the qubits, which might not always be compatible with optimal coherence time conditions, or the implementation of other gates. This is particularly important for qubits with a so-called sweet-spot, an optimal bias point at which the qubit is rendered insensitive to specific noise channels, and coherence times can improve by orders of magnitude. For some qubit types and coupling schemes, these sweet-spots are intrinsically connected to having a transverse coupling. Previous work [5, 6, 21, 36, 39–41] has specifically focused on two-qubit quantum gates that can be fully implemented at sweet-spots.

In this work, we theoretically analyse a CNOT gate based on the selective darkening (SD) method proposed and demonstrated in [39]. This method is for transversely coupled qubits and requires driving two qubits simultaneously with a single frequency, with specific relative amplitudes and phases. The method was developed in the context of superconducting qubits, but can also be used for any other coupled-qubit system with pure transverse coupling [42]. The basic principle of the gate is explained in section 2, for both small and large coupling energies. In section 3, we briefly discuss the relation of SD to other comparable methods. The time-domain evolution of the gate is investigated in section 4, including the possible gate errors caused by ac-Stark shifts due to off-resonant driving of other transitions in the system. A numerical study of the gate evolution, gate errors and gate speed is presented in section 5. The influence of possible higher-lying levels is analysed for weakly anharmonic qubits in section 6. Lastly, the scalability of the method to systems of multiple qubits is studied in section 7, and the paper ends with the conclusions and discussion of the results.

2. Selective darkening

2.1. Basic principle

SD provides an entangling operation between two coupled qubits. To operate the gate, one drives both qubits with a common frequency, but individually tuned amplitudes and phases. In this section, we first give an intuitive explanation of the method, and for simplicity assume a coupling energy between the qubits that is much smaller than the other energies in the system.

The SD method is suitable for any coupled-qubit system where the effective coupling term is purely transverse, i.e. where the matrix describing the interaction, written in the energy eigenbasis of the uncoupled system, does not contain any diagonal elements. Here, we consider a system of two transversely coupled qubits that is described by the Hamiltonian

$$\hat{H}_0 = -\frac{1}{2} (\Delta_1 \hat{\sigma}_z^{(1)} + \Delta_2 \hat{\sigma}_z^{(2)}) + J \hat{\sigma}_x^{(1)} \hat{\sigma}_x^{(2)}, \quad (1)$$

where Δ_i is the single-qubit energy splitting of qubit i , J is the qubit–qubit coupling energy and $\hat{\sigma}_{x,y,z}^{(i)}$ are the Pauli spin matrices ($\hat{\sigma}_{x,y,z}^{(1)} = \hat{\sigma}_{x,y,z} \otimes \mathbb{1}$, $\hat{\sigma}_{x,y,z}^{(2)} = \mathbb{1} \otimes \hat{\sigma}_{x,y,z}$). Note, however, that other (effective) Hamiltonians with pure transverse coupling, i.e. with any combination of $\hat{\sigma}_{x,y}^{(1)} \hat{\sigma}_{x,y}^{(2)}$ coupling terms, would not change the principle of the method. The same remark holds for systems where the coupling is not direct between the two qubits, but mediated by an extra coupling element such as a harmonic oscillator [43] or a superconducting quantum interference device (SQUID) [22]. In figures 1(a) and (b), two relevant example systems are depicted.

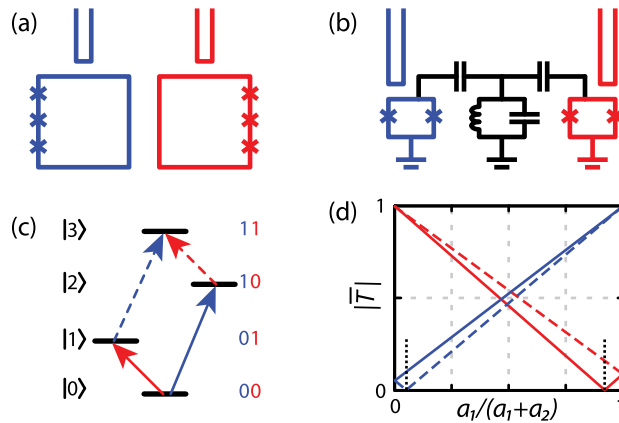


Figure 1. Selective darkening. (a) Schematic diagram of two inductively coupled flux qubits and two antennas for individual driving. (b) Schematic diagram of transmon or charge qubits, coupled via a harmonic oscillator, and with two antennas for individual driving. (c) Energy-level diagram of the coupled qubit system. Arrows of the same colour indicate transitions of the same qubit and are degenerate in frequency. (d) The normalized transition strengths of the four transitions in (c) as a function of the net driving amplitudes $a_1/(a_1+a_2)$ for $\varphi_2 - \varphi_1 = 0$. For $\varphi_2 - \varphi_1 = \pi$ the dashed and solid lines are interchanged. The black dotted lines indicate the condition for which the corresponding transition is darkened.

As a first step, we treat the coupling strength J as a perturbation, taking $J \ll |\Delta_1 - \Delta_2|$. We also assume that $|\Delta_1 - \Delta_2| \ll \Delta_1, \Delta_2$, so that we can ignore terms containing the ratio J/Δ_j . With no loss of generality, we also take $\Delta_1 > \Delta_2$. To first order in perturbation theory, the four energy eigenstates are given by

$$\begin{aligned}
 |0\rangle &= |00\rangle, \\
 |1\rangle &= |01\rangle - \frac{J}{\Delta_1 - \Delta_2} |10\rangle, \\
 |2\rangle &= |10\rangle + \frac{J}{\Delta_1 - \Delta_2} |01\rangle, \\
 |3\rangle &= |11\rangle.
 \end{aligned} \tag{2}$$

The energies are unaffected by the perturbation to first order. In other words, $E_2 - E_0 = E_3 - E_1 = \Delta_1$ and $E_1 - E_0 = E_3 - E_2 = \Delta_2$. (In the next section it is shown that the relations $E_2 - E_0 = E_3 - E_1$ and $E_1 - E_0 = E_3 - E_2$ hold to *any* order.) The energy levels are shown schematically in figure 1(c). The arrows indicate the transitions of interest; the blue and red arrows describe the transitions of qubits 1 and 2, respectively. As mentioned above, each pair of transitions is degenerate, which is typical of transverse coupling⁷. Let us now add a driving term of frequency ω , resonant with one of the degenerate pairs of transitions, that couples with

⁷ For simplicity, we label the states as if the qubits were uncoupled, although the single-qubit states are mixed by the coupling. This state mixing is central to the SD method. Note that in the case of fixed coupling, this state mixing needs to be taken into account when defining a suitable readout scheme.

amplitude a_1 and phase φ_1 to qubit 1 and a_2 and with φ_2 to qubit 2:

$$\begin{aligned}\hat{H}_{\text{drive}} &= a_1 \cos(\omega t + \varphi_1) \hat{\sigma}_x^{(1)} + a_2 \cos(\omega t + \varphi_2) \hat{\sigma}_x^{(2)} \\ &= \tilde{H}_{\text{drive}}^+ e^{i\omega t} + \tilde{H}_{\text{drive}}^- e^{-i\omega t},\end{aligned}\quad (3)$$

where

$$\tilde{H}_{\text{drive}}^\pm = \frac{a_1}{2} e^{\pm i\varphi_1} \hat{\sigma}_x^{(1)} + \frac{a_2}{2} e^{\pm i\varphi_2} \hat{\sigma}_x^{(2)}.\quad (4)$$

The amplitudes a_1 and a_2 are real and positive, and the phases φ_1 and φ_2 are real. If we choose $\omega = \Delta_2/\hbar$ (in our first-order approximation), we match the transition frequency for flipping the state of the second qubit, i.e. we should drive the transitions $|0\rangle \leftrightarrow |1\rangle$ and $|2\rangle \leftrightarrow |3\rangle$ (corresponding to red arrows in figure 1(c)). We now evaluate the transition strengths $T_{k \leftrightarrow l} = \langle l | \tilde{H}_{\text{drive}} | k \rangle$ of both transitions, i.e. the matrix elements that govern the Rabi frequencies of the oscillations ($\omega_R = 2|T|/\hbar$). The term \tilde{H}_{drive} represents the (time-independent) co-rotating field, meaning that we take the rotating wave approximation, giving $\tilde{H}_{\text{drive}} = \tilde{H}_{\text{drive}}^+$ for $k > l$ and $\tilde{H}_{\text{drive}} = \tilde{H}_{\text{drive}}^-$ for $k < l$. (Derivation of the co- and counter-rotating terms is done in appendix A.) The resulting transition strengths are

$$\langle 1 | \tilde{H}_{\text{drive}} | 0 \rangle = -\frac{a_1}{2} \frac{J}{\Delta_1 - \Delta_2} e^{-i\varphi_1} + \frac{a_2}{2} e^{-i\varphi_2},\quad (5a)$$

$$\langle 3 | \tilde{H}_{\text{drive}} | 2 \rangle = +\frac{a_1}{2} \frac{J}{\Delta_1 - \Delta_2} e^{-i\varphi_1} + \frac{a_2}{2} e^{-i\varphi_2}.\quad (5b)$$

Crucially, the two transition strengths are not equal. Figure 1(d) shows the normalized $|\bar{T}| = |T|/(a_1 + a_2)$ as a function of $a_1/(a_1 + a_2)$ for a fixed phase difference $\varphi_2 - \varphi_1 = 0$. The blue lines correspond to the two transitions of qubit 2. The difference in transition strength leads to a different evolution for the two corresponding transitions. This can be conveniently visualized using a Bloch sphere representation, as shown in figure 2(a). The black and grey arrows both represent the state of the qubit that is resonantly driven (in our example, qubit 2), where black (grey) indicates that the other qubit is in state $|0\rangle$ ($|1\rangle$). The transition strength is a complex number and both the amplitude and the phase are relevant for the evolution of the state. Difference in the *amplitudes* of the two transition strengths leads to different Rabi frequencies of the oscillations ($\omega_{R,1} \neq \omega_{R,2}$). Difference in the *phases* of the transition strengths leads to different rotation axes ($\varphi_{R,1} \neq \varphi_{R,2}$).

We now make some simple observations. A single-qubit gate is a gate that changes the state of one qubit with the change being independent of the state of the other qubit(s). In the Bloch sphere picture this means that when a rotation is induced on one qubit, the rotation speed and the orientation of the rotation axis do not depend on the other qubit being in state $|0\rangle$ or $|1\rangle$. This situation is indicated in figure 2(d). This occurs only when the driving field couples exclusively to the qubit that is resonant with the driving field; in our case this corresponds to $a_1 = 0$ (or $a_1/(a_1 + a_2) = 0$, see figure 1(c)). *All other settings of the driving field lead to entangling evolution of the system, and can be used to create entangling gates.* Note that if one intends to perform a single-qubit gate, and the drive is not applied exclusively to that qubit, the two-qubit evolution that is aimed at in this work should be taken into account as a possible source of errors, unless the system has a tunable coupling that can be reduced to zero [16, 24, 44].

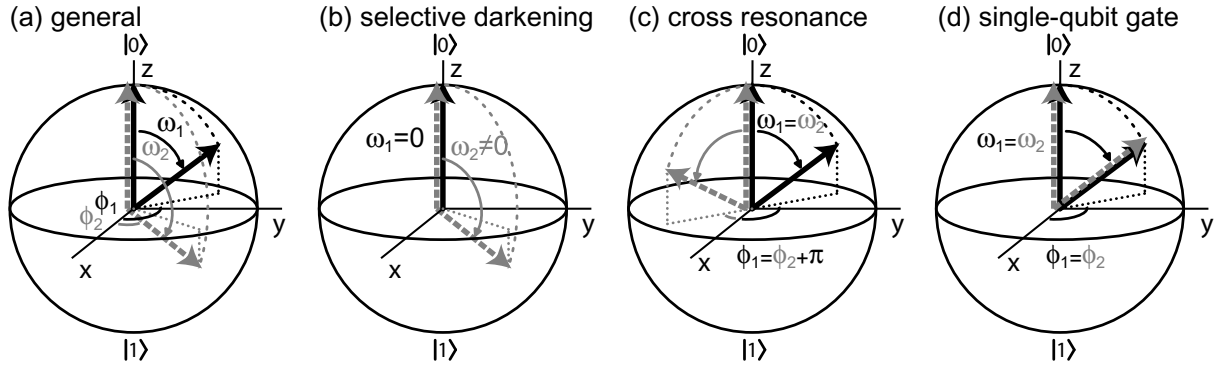


Figure 2. Bloch sphere representation of the evolution of a resonantly driven degenerate transition for different driving conditions. The black and grey arrows show the evolution of the state of the target qubit, for the control qubit in state $|0\rangle$ and state $|1\rangle$, respectively. (a) The general case. The two state vectors rotate with different Rabi frequencies and around different axes. (b) Selective darkening. Rotation of one of the state vectors is fully suppressed. The other state vector has a non-zero Rabi frequency. (c) Cross resonance. The state vectors rotate around the same axis, with equal Rabi frequency but in opposite directions. (d) Single-qubit gate. The state vectors rotate around the same axis, with equal Rabi frequency and in the same direction.

Even though many different settings of the driving field can be used to create entangling gates, two special cases stand out. The first is where the driving field resonant with one qubit is exclusively applied to the non-resonant qubit ($a_2 = 0$, $a_1/(a_1 + a_2) = 1$). This driving scenario will lead to equal rotation speed of both state vectors, but opposite direction. This case will be discussed further in section 3.

The second special case is the main focus of this paper, where one of the transition strengths is equal to zero (depicted in figure 1(d) by the black dotted lines). Here one transition is fully suppressed, i.e. darkened, while the other transition has a finite transition strength. Specifically, if we choose

$$\frac{a_2}{a_1} = \frac{J}{\Delta_1 - \Delta_2}, \quad (6)$$

and $\varphi_2 - \varphi_1 = 0$, we find that the Rabi oscillation frequency for the transition $|0\rangle \leftrightarrow |1\rangle$ is zero, so that we only drive the transition $|2\rangle \leftrightarrow |3\rangle$. This condition provides exactly what is required for a CNOT gate: for the appropriate driving duration the state of the second qubit is flipped if the first qubit is in state $|1\rangle$, whereas it remains unaffected if the first qubit is in state $|0\rangle$. The 0-CNOT gate, where the second qubit is flipped only if the first qubit is in state $|0\rangle$, is achieved by taking equation (6) and $\varphi_1 - \varphi_2 = \pi$.

The speed of the gate is determined by the transition strength of the non-darkened transition, which is now given by

$$\langle 3 | \tilde{H}_{\text{drive}} | 2 \rangle = a_2 = a_1 \frac{J}{\Delta_1 - \Delta_2}. \quad (7)$$

One must take care that both a_1 and a_2 are small enough to not excite other transitions by off-resonant excitation. As a simple estimation of the maximum gate speed, we take the driving

amplitudes such that for all the off-resonant transitions the transition strength is smaller than the detuning of the transition frequency with the driving field: $\langle l | \tilde{H}_{\text{drive}} | k \rangle < |\hbar\omega - \hbar\omega_{l \leftrightarrow k}|$. In this case the transitions $|0\rangle \leftrightarrow |2\rangle$ and $|1\rangle \leftrightarrow |3\rangle$ provide the tightest restrictions ($\langle 2 | \tilde{H}_{\text{drive}} | 0 \rangle \approx \langle 3 | \tilde{H}_{\text{drive}} | 1 \rangle \approx a_1/2$), giving $a_1/2 < (\Delta_1 - \Delta_2)$. The resulting estimate for the maximum Rabi frequency of the CNOT transition is

$$\omega_{R,\text{max}} \sim 4J/\hbar. \quad (8)$$

This means that the maximum gate speed is determined by J , which is the fundamental upper limit on performing a two-qubit gate; a two-qubit gate cannot be faster than the coupling strength in the system [45]. How close the gate can get to this estimate for the maximum speed (for a given fidelity) is studied numerically in section 5.

2.2. Strong coupling

In the simplified calculations of the previous subsection, the energy eigenstates are easily identifiable as being almost equal to the states of the computational basis. However, the Hamiltonian (equation (1)) is simple enough that it can be diagonalized without approximations:

$$\begin{aligned} |0\rangle &= \cos(\theta_1/2) |00\rangle - \sin(\theta_1/2) |11\rangle, \\ |1\rangle &= \cos(\theta_2/2) |01\rangle - \sin(\theta_2/2) |10\rangle, \\ |2\rangle &= \cos(\theta_2/2) |10\rangle + \sin(\theta_2/2) |01\rangle, \\ |3\rangle &= \cos(\theta_1/2) |11\rangle + \sin(\theta_1/2) |00\rangle, \end{aligned} \quad (9)$$

where

$$\tan \theta_1 = \frac{2J}{\Delta_1 + \Delta_2}, \quad \tan \theta_2 = \frac{2J}{\Delta_1 - \Delta_2}. \quad (10)$$

For compactness of the following equations, we also define

$$\theta_+ = \frac{\theta_1 + \theta_2}{2}, \quad \theta_- = \frac{\theta_2 - \theta_1}{2}. \quad (11)$$

We now find that

$$\langle 1 | \tilde{H}_{\text{drive}} | 0 \rangle = -\frac{a_1}{2} e^{-i\varphi_1} \sin \theta_+ + \frac{a_2}{2} e^{-i\varphi_2} \cos \theta_-, \quad (12a)$$

$$\langle 3 | \tilde{H}_{\text{drive}} | 2 \rangle = +\frac{a_1}{2} e^{-i\varphi_1} \sin \theta_+ + \frac{a_2}{2} e^{-i\varphi_2} \cos \theta_-, \quad (12b)$$

and

$$\langle 2 | \tilde{H}_{\text{drive}} | 0 \rangle = \frac{a_1}{2} e^{-i\varphi_1} \cos \theta_+ + \frac{a_2}{2} e^{-i\varphi_2} \sin \theta_-, \quad (12c)$$

$$\langle 3 | \tilde{H}_{\text{drive}} | 1 \rangle = \frac{a_1}{2} e^{-i\varphi_1} \cos \theta_+ - \frac{a_2}{2} e^{-i\varphi_2} \sin \theta_-. \quad (12d)$$

The condition for SD of qubit 2 transitions is then given by

$$\frac{a_2}{a_1} = \frac{\sin \theta_+}{\cos \theta_-}, \quad (13)$$

with $\varphi_2 - \varphi_1 = 0$ for the 1-controlled CNOT gate (1-CNOT) and $\varphi_2 - \varphi_1 = \pi$ for the 0-CNOT gate. This condition generalizes equation (6), which was derived for the weak-coupling limit. The condition for SD of qubit 1 transitions is

$$\frac{a_2}{a_1} = \frac{\cos \theta_+}{\sin \theta_-}, \quad (14)$$

with $\varphi_2 - \varphi_1 = \pi$ for the 1-CNOT gate and $\varphi_2 - \varphi_1 = 0$ for the 0-CNOT gate. In this case (i.e. with arbitrary values of Δ_1 , Δ_2 and J), the transition frequencies are given by

$$E_1 - E_0 = E_3 - E_2 = \frac{1}{2} \left(\sqrt{4J^2 + (\Delta_1 + \Delta_2)^2} - \sqrt{4J^2 + (\Delta_1 - \Delta_2)^2} \right), \quad (15a)$$

$$E_2 - E_0 = E_3 - E_1 = \frac{1}{2} \left(\sqrt{4J^2 + (\Delta_1 + \Delta_2)^2} + \sqrt{4J^2 + (\Delta_1 - \Delta_2)^2} \right). \quad (15b)$$

Note that this derivation shows that the SD gate can also be used when $\Delta_1 = \Delta_2$, giving $a_1 = a_2$ for the required amplitude ratio for both qubit 1 or 2 as the target qubit. In this special case, the SD method is equivalent to the method proposed by Beige *et al* [46] and has recently been demonstrated experimentally [47].

3. Relation to other gates

Independently of our work on SD, a cross resonance (CR) scheme for realizing two-qubit gates for transversely coupled qubits was proposed in [40]. The CR coupling scheme relies on driving one qubit (the control qubit) at the resonance frequency of the other qubit (the target qubit) and has the result of driving Rabi oscillations in the target qubit in one of two opposite directions based on the state of the control qubit. Even though at first sight the driving condition and resulting dynamics might seem to be very different from those of the SD scheme, the two schemes are related by a simple rotation. This relation can be inferred from figures 2(b) and (c) and by noting that in both cases the two-qubit dynamics involve rotations of the target-qubit state about a single axis. As a result, the two-qubit evolution commutes with any single-qubit rotation about the same axis. One can therefore convert any CR-like operation into an SD-like operation by applying a single-qubit rotation designed to cancel one of the two possible CR rotations. Crucially, because the single-qubit and two-qubit rotations commute, they can be applied simultaneously. Starting from the CR scheme as a reference point, one could say that the driving field applied to the target qubit in the SD scheme is designed to oppose one of the two rotations in the CR scheme, thus producing CNOT-gate dynamics.

It is interesting in this context to look further back into the history of coupling schemes for superconducting qubits. After the proposal of the FLICFORQ coupling scheme [5], it was shown that this scheme is a special case of a family of coupling schemes using the physics of double resonance [36, 37]. In particular, even though the coupling scheme used in [38] might seem very different from FLICFORQ, they are both special cases of the double-resonance family of coupling schemes. The general condition that needs to be satisfied for double resonance is given by

$$\pm \sqrt{(\hbar\omega_1 - \Delta_1)^2 + a_1^2} \pm \sqrt{(\hbar\omega_2 - \Delta_2)^2 + a_2^2} = \hbar\omega_1 - \hbar\omega_2. \quad (16)$$

It is interesting to note that the condition for the CR [40] and SD gates [39], i.e. driving both qubits at the frequency of one of them with small amplitudes, satisfies the double-resonance

condition. One can then wonder whether these coupling schemes can also be seen as two more (closely related) members of the double-resonance family.

The CR and SD schemes can indeed be seen as special cases of double resonance. However, they also involve some qualitative differences to the previously studied cases, such as the FLICFORQ and ac-Stark-shift-induced resonance, making them more like distant relatives of the conventional double-resonance schemes. (It is worth noting here that another different scheme of the same family was discovered in the numerical results in [37]). One difference between the more conventional double-resonance schemes and the CR and SD schemes becomes apparent if one plots the energy-level diagrams of the two driven qubits in the dressed-state picture. In the schemes of [5, 38], one transition between dressed states of qubit 1 becomes resonant with one transition between dressed states of qubit 2. As a result, a swap-like operation takes place with the two single-qubit transitions driven in opposite directions, such that the total energy is conserved. In the case of CR and SD, two pairs of transitions are resonant and are involved in the gate operation, as can be seen from figures 1 and 4 of [40]. The result turns out to be a conditional operation: the well-known CNOT-gate dynamics in the SD case and a CNOT gate combined with a single-qubit rotation in the CR case.

Classification of different gates can also be done using the geometric representation of [1, 48, 49]. Being related by simple single-qubit gates, the CR and SD-CNOT gates correspond to exactly the same dynamics of the Makhlin parameters. The more conventional double-resonance class of gates, as well as the gate of [50], all exhibit oscillations corresponding to the *i*SWAP gate. As a result, the Makhlin parameters exhibit similar behaviour for these cases.

In [51], a scheme is discussed to control the individual states in degenerate subspaces of three qubits coupled in a loop. That scheme is based on the same principles as the SD and CR methods. The gate proposed in [50] is similar to the CR and SD methods in the sense that it also provides a microwave-only entangling gate between two qubits and does not involve shifting the dressed states into resonance by strong driving. This gate, however, requires a coupling type that is at least partially longitudinal. Creating entangling evolution between two coupled qubits by tuning the amplitudes and phases of a driving field is also discussed in [52, 53].

Another intimately related effect to SD is illustrated by the *dark states* encountered in circuit quantum electrodynamics. When two qubits are both coupled to a harmonic oscillator and the qubits are biased to have equal splitting, the energy levels exhibit an anti-crossing. Some of the transitions are typically found to be forbidden. This effect can be interpreted as SD, as the condition for SD to occur for two qubits of equal splitting is when both the qubits are driven with equal amplitude [47] (see section 2.2). Recently, it was proposed and demonstrated that these properties can be exploited further by defining a new logical qubit from two conventional qubits, using only two of the four original states [54–56]. Within this definition, the coupling to the resonator can be treated as tunable, and the qubit itself can be shielded from decay through the resonator.

4. Time-domain evolution of the gate and spurious driving of other transitions

To compare different methods for creating entangling gates or to design the optimum parameters for a certain experiment, it is important to know the potential sources of errors and how these errors depend on the various parameters in the system. The first potential source of errors that we study is related to the ac-Stark effect, i.e. the energy shift that the driving field can induce on the non-resonant transitions in the system. Specifically, the applied driving field is resonant

with the qubit that is to be flipped (the target qubit of the CNOT gate), but the same field also drives the control qubit, which typically has a different transition frequency. This off-resonant driving leads to a predictable but unwanted deviation from the pure CNOT-type evolution of the system.

4.1. Ideal gate evolution under rotating wave approximation

The time evolution of the system is best studied in a suitable rotating frame. In this case, the driving term \hat{H}_{drive} in equation (3) can be conveniently split into a (time-independent) co-rotating term \tilde{V} and a (time-dependent) counter-rotating term \tilde{W} (see appendix A). For the co-rotating term \tilde{V} , we find the matrix elements given in equations (12a)–(12d) with $\tilde{H}_{\text{drive}} = \tilde{V}$.

We now make the rotating wave approximation: the counter-rotating term \tilde{W} oscillates very fast (at frequency 2ω) and is therefore approximated by its average value, zero. The gate we would like to perform is the usual CNOT gate, with qubit 2 as the target qubit. We therefore choose

$$\begin{aligned} \hbar\omega &= E_3 - E_2 = E_1 - E_0 \\ &= \frac{1}{2} \left(\sqrt{(\Delta_1 + \Delta_2)^2 + 4J^2} - \sqrt{(\Delta_1 - \Delta_2)^2 + 4J^2} \right), \end{aligned} \quad (17a)$$

$$\frac{a_2}{a_1} = \frac{\sin \theta_+}{\cos \theta_-}, \quad (17b)$$

$$\varphi_2 - \varphi_1 = 0. \quad (17c)$$

We are now left with

$$\tilde{H}_0 = \frac{1}{2} \sqrt{(\Delta_1 - \Delta_2)^2 + 4J^2} \begin{pmatrix} -1 & 0 & 0 & 0 \\ 0 & -1 & 0 & 0 \\ 0 & 0 & 1 & 0 \\ 0 & 0 & 0 & 1 \end{pmatrix}, \quad (18)$$

$$\begin{aligned} \langle 1 | \tilde{V} | 0 \rangle &= 0, \\ \langle 2 | \tilde{V} | 0 \rangle &= \frac{a_1}{2} (\cos \theta_+ + \sin \theta_+ \tan \theta_-) e^{-i\varphi_1}, \\ \langle 3 | \tilde{V} | 2 \rangle &= a_1 \sin \theta_+ e^{-i\varphi_1}, \\ \langle 3 | \tilde{V} | 1 \rangle &= \frac{a_1}{2} (\cos \theta_+ - \sin \theta_+ \tan \theta_-) e^{-i\varphi_1}, \\ \langle i | \tilde{V} | j \rangle &= \langle j | \tilde{V} | i \rangle^*. \end{aligned} \quad (19)$$

In a first approximation, we ignore the matrix elements \tilde{V}_{20} and \tilde{V}_{31} (and their Hermitian conjugates). We then find the effective Hamiltonian

$$\tilde{H} = \tilde{H}_0 + \begin{pmatrix} 0 & 0 & 0 & 0 \\ 0 & 0 & 0 & 0 \\ 0 & 0 & 0 & \tilde{V}_{32}^* \\ 0 & 0 & \tilde{V}_{32} & 0 \end{pmatrix}. \quad (20)$$

These two terms commute, and their effects can be easily superimposed. If the Hamiltonian is allowed to operate for a time $t = h/(4|\tilde{V}_{32}|) = h/(4a_1 \sin \theta_+)$, the first term produces the transformation

$$\begin{pmatrix} e^{i\sqrt{(\Delta_1-\Delta_2)^2+4J^2}t/2} & 0 & 0 & 0 \\ 0 & e^{i\sqrt{(\Delta_1-\Delta_2)^2+4J^2}t/2} & 0 & 0 \\ 0 & 0 & e^{-i\sqrt{(\Delta_1-\Delta_2)^2+4J^2}t/2} & 0 \\ 0 & 0 & 0 & e^{-i\sqrt{(\Delta_1-\Delta_2)^2+4J^2}t/2} \end{pmatrix}, \quad (21)$$

and the second term produces the transformation

$$\begin{pmatrix} 1 & 0 & 0 & 0 \\ 0 & 1 & 0 & 0 \\ 0 & 0 & 0 & -ie^{-i\varphi_1} \\ 0 & 0 & -ie^{i\varphi_1} & 0 \end{pmatrix}. \quad (22)$$

These transformations are given in the rotating frame. They can be transformed back to the laboratory frame to give

$$\begin{pmatrix} e^{-iE_0t} & 0 & 0 & 0 \\ 0 & e^{-iE_1t} & 0 & 0 \\ 0 & 0 & e^{-iE_2t} & 0 \\ 0 & 0 & 0 & e^{-iE_3t} \end{pmatrix} \begin{pmatrix} 1 & 0 & 0 & 0 \\ 0 & 1 & 0 & 0 \\ 0 & 0 & 0 & -ie^{-i\varphi_1} \\ 0 & 0 & -ie^{i\varphi_1} & 0 \end{pmatrix}. \quad (23)$$

The leftmost matrix represents the Larmor precession of the system in the laboratory frame. Taking $\varphi_1 = 0$, the rightmost matrix is exactly the CNOT gate, up to a single-qubit phase gate and a global phase factor (meaning that the Makhlin parameters [48] are equal to those of the standard CNOT gate).

4.2. Single- and two-qubit errors caused by the ac-Stark effect

We now include the two (or four including the conjugate terms) matrix elements that we have ignored in the previous subsection:

$$\langle 2|\tilde{V}|0\rangle = \frac{a_1}{2} (\cos \theta_+ + \sin \theta_+ \tan \theta_-) e^{-i\varphi_1}, \quad (24a)$$

$$\langle 3|\tilde{V}|1\rangle = \frac{a_1}{2} (\cos \theta_+ - \sin \theta_+ \tan \theta_-) e^{-i\varphi_1}. \quad (24b)$$

These matrix elements produce an ac-Stark shift on qubit 1 (the control qubit). If θ_+ and θ_- are small, the above two matrix elements are approximately equal to $a_1/2$ (up to a phase factor). This matrix element then causes a shift of $a_1^2/2(E_2 - E_0 - \hbar\omega)$. This frequency shift can be incorporated easily into the transformation given in equations (A.3)–(A.7), simply modifying the energies that enter equation (A.1).

Note, however, that the two matrix elements above are slightly different, so that the ac-Stark shift of qubit 1 depends on the state of qubit 2. This situation would induce an unwanted controlled-phase (CPHASE) gate. If we take $\Delta_1/h = 6$ GHz, $\Delta_2/h = 5$ GHz and $J/h = 0.1$ GHz, we find that $\theta_1 = 0.0058\pi$ and $\theta_2 = 0.063\pi$, which gives the ratio between the matrix elements:

$$\frac{\langle 2|\tilde{V}|0\rangle}{\langle 3|\tilde{V}|1\rangle} = \frac{\cos \theta_+ + \sin \theta_+ \tan \theta_-}{\cos \theta_+ - \sin \theta_+ \tan \theta_-} = 1.02. \quad (25)$$

This means that for the given parameters, the two different values for the ac-Stark shift will differ by about 4%. This 4% difference of the frequency shift should therefore be designed such that it causes an overall phase shift much smaller than 2π over the gate time of typically a few nanoseconds. It can then be neglected. Otherwise, it could harm the fidelity of the gate. Even for extremely strong driving ($a_1/h = 1$ GHz), which gives a large ac-Stark shift (about 0.5 GHz), over a gate time of 4 ns, we obtain an unwanted CPHASE rotation by an angle of 0.16π . For weaker driving this unwanted angle will be smaller.

Note that in our case, this CPHASE-type error can also be corrected relatively easily using single-qubit gates. In this case the SD-CNOT part of the gate is intentionally made to deviate slightly from a perfect CNOT gate by using a longer or shorter gate time, such that the evolution of the state-vector overshoots or undershoots the normal π -rotation. If the correction to the gate time is chosen appropriately, the combined evolution of the unwanted CPHASE gate and the intentionally driven CNOT gate can be transformed into a perfect CNOT gate using single-qubit gates before and after the two-qubit driving. This effect is related to the well-known fact that a CPHASE gate can be transformed into a CNOT gate using only single-qubit gates [57]. This type of correction will be demonstrated in section 5.

A more rigorous analysis (see appendix B), where the driving field is treated quantum mechanically, confirms the single-qubit and two-qubit errors found here. In addition, even though we mostly look at the high driving limit where the classical description of the field gives accurate results, some phenomena can be identified more easily. Specifically, it is shown that for increasing amplitudes of the driving field not only the levels of the control qubit are shifted, but also the transitions of the target qubit are no longer perfectly degenerate. In this case no transition can be fully darkened. The result is a single-qubit-type error on the target qubit. As mentioned above, single-qubit errors can be corrected relatively easily. It should be noted, however, that this error can slow down the CNOT gate. A perfect SD-CNOT gate requires the state vectors in the example of figure 2 to be on opposite sides of the Bloch sphere at the end of the gate, and co-rotation of the transition that should be darkened leads to a saturation of the effective gate speed. This will also be considered in section 5.

5. Numerical simulation of gate dynamics for two-level qubits

To quantify the fidelity of the SD-CNOT gate, the evolution of the system was simulated numerically. We take the driving conditions derived from the simple weak driving case given in section 2: the frequency of the driving field was chosen to be $\omega = (E_1 - E_0)/\hbar = (E_3 - E_2)/\hbar$, and the amplitude ratio as given in equation (13). The amplitudes are ramped up and down using the half-sine envelope function $\sin(\pi t/t_{\text{gate}})$, with t running from 0 to the total gate time t_{gate} . Note that we chose to gradually turn on and off the driving field rather than using step functions, because in many cases the steep edges can lead to undesired excitations in the system. This approach increases the gate time with a factor of $\pi/2$ compared to the minimum gate time where the driving amplitude is turned on and off abruptly. Other envelope shapes would give similar correction factors.

For a given maximum amplitude a_1 , the evolution of the system was simulated. The evolution operator at the end of the gate was evaluated according to its overlap with the ideal CNOT gate, which is quantified using the fidelity $\mathcal{F} = \text{Tr}(M_{\text{gate}}M_{\text{CNOT}})/4$. Here M_{gate} is the (unitary) matrix of the simulated gate and M_{CNOT} the ideal CNOT gate from equation (23) (which includes the phase factors i). This calculation is performed for 20 different gate

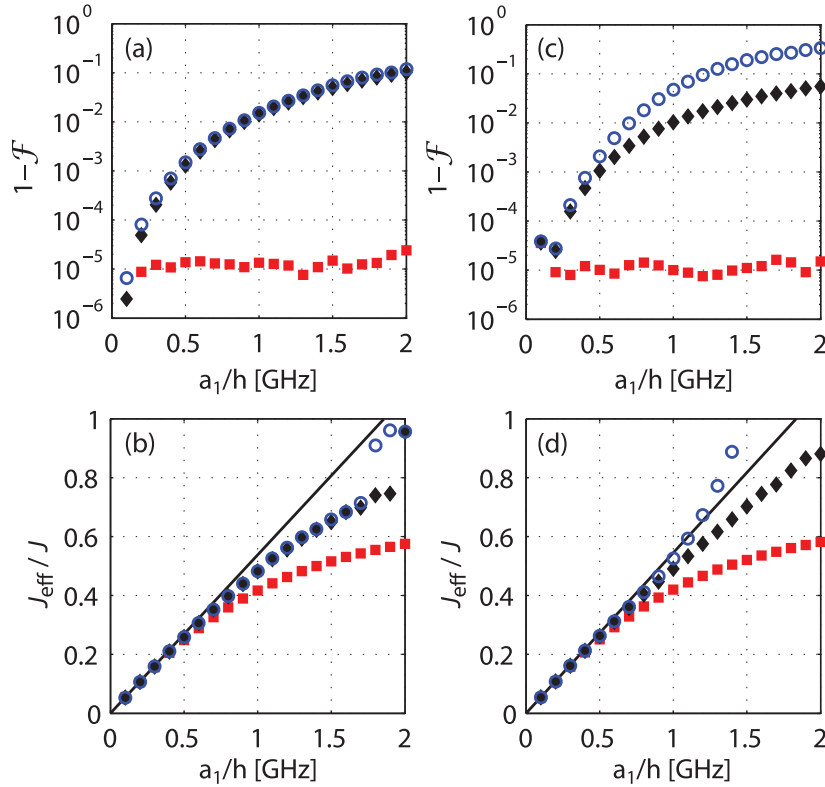


Figure 3. Numerical simulation of an SD-CNOT gate for two-level qubits. Panels (a) and (b) are calculated for coupling strengths of $J/h = 100$ MHz and (c) and (d) for $J/h = 25$ MHz. Blue circles represent the results for the SD-CNOT gate, incorporating only corrections for Larmor precession and ac-Stark shift of the control qubit. The other two data sets represent the SD-CNOT gate including error corrections using single-qubit phase gates (black diamonds) and arbitrary single-qubit gates (red squares). In panels (a) and (c), the gate error $1 - \mathcal{F}$ is plotted against the driving strength. Panels (b) and (d) give the corresponding gate speed, expressed as the effective coupling strength J_{eff} divided by the natural coupling strength, for which fidelity \mathcal{F} is achieved. The black lines indicate the expected dependence from equations (12a)–(12d). The values used for the qubit splittings are $\Delta_1/h = 6$ GHz and $\Delta_2/h = 5$ GHz.

times around an estimated optimum. An interpolating polynomial function was used to fit the dependence of the fidelity on the gate time, providing the final accurate estimate for the optimum gate time. The gate was recalculated using this gate time, giving the final result for the fidelity. This sequence is repeated for different driving amplitudes a_1 (with a_2 adjusted to the ratio given in equation (13)). The qubit splittings used are $\Delta_1/h = 6$ GHz and $\Delta_2/h = 5$ GHz and the phases of the driving fields are $\varphi_1 = \varphi_2 = 0$.

The results of the simulations are shown in figure 3. Figures 3(a) and (b) were calculated for a coupling strength $J/h = 100$ MHz, and figures 3(c) and (d) for $J/h = 25$ MHz. The blue circles give the result of the procedure as described above, using the lowest number of corrections. We only take into account the Larmor precession and for the control qubit the ac-Stark and Bloch–Siegert shift due to the (off-resonant) driving, disregarding for the

level shifts any effects related to the coupling. The bare SD-CNOT gate is calculated first and the corrections are applied afterwards as phase gates. The required phase for the ac-Stark and Bloch–Siegert shift corrections is calculated analytically from the energy shifts $\delta E_{\text{ac-Stark}} = a_1^2/2(E_2 - E_0 - \hbar\omega)$ and $\delta E_{\text{Bloch-Siegert}} = a_1^2/2(E_2 - E_0 + \hbar\omega)$ and the gate time t_{gate} , taking into account the envelope shape. The correction for the Larmor precession is given by the conjugate of the leftmost matrix in equation (23). Note, however, that all these corrections often do not have to be implemented physically in an experiment. The internal phase evolution of a microwave source that is set to the resonance frequency will automatically follow the Larmor precession of the qubit, and a single-qubit phase gate can often be incorporated easily in the preceding or following single-qubit gates.

For the black diamonds and red squares we performed the same procedure, but in addition we allowed single-qubit phase gates (black diamonds) or arbitrary single-qubit rotations (red squares) before and after the two-qubit gate. For each simulation of the two-qubit gate an optimization algorithm is used to find the single-qubit gates that optimize the fidelity of the gate. This approach allows for correcting certain error types, such as the CPHASE-type error discussed in section 4.2. Note that in all three cases, the corrections influence not only the maximum fidelity of the gate, but also for which t_{gate} the maximum is found.

We characterized the gate speed as the effective coupling strength $J_{\text{eff}} = h/t_{\text{gate}} \cdot \pi/2$, where the factor $\pi/2$ takes into account the envelope function of the driving field. In figures 3(b) and (d), the black lines represent the expected gate speed as given in equations (12a)–(12d). For low driving strengths the gate speed follows exactly the linear behaviour as expected from the transition strength. The gate error (given by $1 - \mathcal{F}$), increases monotonically with driving strength, except for the case with arbitrary single-qubit corrections where the error is $\sim 10^{-5}$ throughout the whole range and is limited only by the accuracy of the numerical calculation. The low error in the latter case shows that the errors in the SD-CNOT gate are either single-qubit errors or two-qubit errors that can be incorporated into the combined evolution to form a perfect CNOT gate, such as the CPHASE-type errors discussed in section 4.2. Also, in experiment this would be an attractive way to enhance the gate performance.

The slowdown of the gate for the results with arbitrary single-qubit gates (red squares) at higher driving frequencies can be explained by the error types discussed in the previous sections. If the transition $|0\rangle \leftrightarrow |1\rangle$ is not fully darkened and the state vector rotates in the same direction as the $|2\rangle \leftrightarrow |3\rangle$ (CNOT) transition, a longer gate time is required to achieve maximum separation of the two state vectors (to achieve a perfect CNOT gate the alignment of the two state vectors should be exactly opposite). Alternatively, a CPHASE-type error can require a slight overshoot of the CNOT gate evolution to achieve the best fidelity when including the single-qubit gates. Both processes are likely to contribute to the observed slowdown of the gate.

At higher driving strengths the gate speed starts to deviate from the linear dependence of the weak-driving limit. In particular, where the error is larger than 0.1, the gate fidelity becomes less well behaved. For $J = 25$ MHz, the effective coupling strength even seems to exceed the natural coupling strength, but this can be explained simply by the fact that the performed gate is no longer close to the desired gate. Also for $J = 25$ MHz, we see an improvement when using the single-qubit phase corrections (black diamonds).

Even without the extra gate optimizations (blue circles), we find a high fidelity at relatively high gate speeds. For the coupling strength of $J = 100$ MHz, gate speeds corresponding to $0.48J$ and $0.07J$ give a gate fidelity of 99% and 99.99% respectively. The exact numbers will depend on the system parameters. Note that these results were obtained using a fixed driving

frequency and amplitude ratio, obtained from simple analytic equations, and using a fixed pulse shape. Using more advanced optimization schemes, for example using the derivative removal by adiabatic gate (DRAG) method [58, 59], these numbers can probably be enhanced further.

6. Weakly anharmonic qubits

The above analysis of the SD-CNOT gate and the possible errors is accurate for true two-level qubits. However, many qubit implementations are in fact multi-level systems. In this case, a nonlinear level structure allows the system to be used as an *effective* two-level system, where only two out of a manifold of levels are used as the (computational) qubit states. When dealing with weakly anharmonic qubits, i.e. qubits where the transition frequencies between consecutive energy levels differ only slightly, the additional energy levels have to be taken into account, as they can significantly influence the dynamics of the system. For example, one obvious complication that arises in this case is the leakage to these additional states.

We take the computational basis to be formed by the lowest two energy states of the qubits, labelled $|00\rangle$, $|01\rangle$, $|10\rangle$ and $|11\rangle$, and the states outside the computational basis are labelled $|02\rangle$, $|20\rangle$, etc. Taking into account the third level of each qubit, and making the approximation of weak coupling ($J \ll \Delta_1 - \Delta_2$) and weak anharmonicity ($\delta_j \equiv \hbar\omega_{1\leftrightarrow 2;j} - \hbar\omega_{0\leftrightarrow 1;j} \ll \Delta_1 - \Delta_2$; note that under this definition δ_j is negative for phase and transmon qubits and positive for capacitively shunted flux qubits), we find the following approximate expressions for the energy eigenstates:

$$\begin{aligned}
 |0\rangle &= |00\rangle, \\
 |1\rangle &= |01\rangle - \frac{J}{\Delta_1 - \Delta_2} |10\rangle, \\
 |2\rangle &= |10\rangle + \frac{J}{\Delta_1 - \Delta_2} |01\rangle, \\
 |3\rangle &= |11\rangle + \frac{\sqrt{2}J}{\Delta_1 - \Delta_2 - \delta_2} |02\rangle - \frac{\sqrt{2}J}{\Delta_1 - \Delta_2 + \delta_1} |20\rangle, \\
 |4\rangle &= |02\rangle - \frac{\sqrt{2}J}{\Delta_1 - \Delta_2 - \delta_2} |11\rangle, \\
 |5\rangle &= |20\rangle + \frac{\sqrt{2}J}{\Delta_1 - \Delta_2 + \delta_1} |11\rangle, \\
 |6\rangle &= |12\rangle + \frac{2J}{\Delta_1 - \Delta_2 - \delta_1 - \delta_2} |21\rangle, \\
 |7\rangle &= |21\rangle + \frac{2J}{\Delta_1 - \Delta_2 + \delta_1 - \delta_2} |12\rangle, \\
 |8\rangle &= |22\rangle.
 \end{aligned} \tag{26}$$

The respective approximate energies are given by

$$\begin{aligned}
 E_0 &= -\frac{\Delta_1}{2} - \frac{\Delta_2}{2}, \\
 E_1 &= -\frac{\Delta_1}{2} + \frac{\Delta_2}{2} - \frac{J^2}{\Delta_1 - \Delta_2},
 \end{aligned}$$

$$\begin{aligned}
E_2 &= +\frac{\Delta_1}{2} - \frac{\Delta_2}{2} + \frac{J^2}{\Delta_1 - \Delta_2}, \\
E_3 &= +\frac{\Delta_1}{2} + \frac{\Delta_2}{2} + \frac{2J^2}{\Delta_1 - \Delta_2 - \delta_2} - \frac{2J^2}{\Delta_1 - \Delta_2 + \delta_1}, \\
E_4 &= -\frac{\Delta_1}{2} + \frac{3\Delta_2}{2} + \delta_2 - \frac{2J^2}{\Delta_1 - \Delta_2 - \delta_2}, \\
E_5 &= +\frac{3\Delta_1}{2} - \frac{\Delta_2}{2} + \delta_1 + \frac{2J^2}{\Delta_1 - \Delta_2 + \delta_1}, \\
E_6 &= +\frac{\Delta_1}{2} + \frac{3\Delta_2}{2} + \delta_2 - \frac{4J^2}{\Delta_1 - \Delta_2 + \delta_1 - \delta_2}, \\
E_7 &= +\frac{3\Delta_1}{2} + \frac{\Delta_2}{2} + \delta_1 + \frac{4J^2}{\Delta_1 - \Delta_2 + \delta_1 - \delta_2}, \\
E_8 &= +\frac{3\Delta_1}{2} + \frac{3\Delta_2}{2}.
\end{aligned} \tag{27}$$

Note that the labels are ordered for increasing energy of the states, except for the interchange of labels 3 and 4. This interchange causes states 0–3 to correspond to the two-level qubit case and makes it easier to compare the two cases.

Let us consider the CNOT gate with qubit 2 being the target qubit. In the qubit basis, this means that the $|0\rangle \rightarrow |1\rangle$ transition is to be darkened, and the $|2\rangle \rightarrow |3\rangle$ transition provides the CNOT gate dynamics. The required relation between the driving amplitudes is again given by equation (6) and $\varphi_2 - \varphi_1 = 0$. For simplicity, in the expressions we also take $\varphi_1 = \varphi_2 = 0$. The transition strengths of the darkened and CNOT-gate transition are now given by

$$\langle 1 | \frac{a_1}{2} \hat{\sigma}_x^{(1)} + \frac{a_2}{2} \hat{\sigma}_x^{(2)} | 0 \rangle \approx \frac{a_1}{2} \left(-\frac{J}{\Delta_1 - \Delta_2} + \frac{J}{\Delta_1 - \Delta_2} \right) = 0, \tag{28a}$$

$$\begin{aligned}
\langle 3 | \frac{a_1}{2} \hat{\sigma}_x^{(1)} + \frac{a_2}{2} \hat{\sigma}_x^{(2)} | 2 \rangle &\approx \frac{a_1}{2} \left(\left[-\frac{2J}{\Delta_1 - \Delta_2 + \delta_1} + \frac{J}{\Delta_1 - \Delta_2} \right] + \frac{J}{\Delta_1 - \Delta_2} \left[1 + \frac{2J^2}{(\Delta_1 - \Delta_2)^2} \right] \right) \\
&\approx a_1 \frac{J}{\Delta_1 - \Delta_2} \left(\frac{\delta_1}{\Delta_1 - \Delta_2} + \frac{J^2}{(\Delta_1 - \Delta_2)^2} \right),
\end{aligned} \tag{28b}$$

where $\hat{\sigma}_x^{(1)} = \hat{\sigma}_x \otimes \mathbb{1}$ and $\hat{\sigma}_x^{(2)} = \mathbb{1} \otimes \hat{\sigma}_x$ are redefined using

$$\hat{\sigma}_x = \begin{pmatrix} 0 & 1 & 0 \\ 1 & 0 & \sqrt{2} \\ 0 & \sqrt{2} & 0 \end{pmatrix}. \tag{29}$$

From these equations we can recognize the first consequence of the additional levels: the transition strength of the $|3\rangle \leftrightarrow |2\rangle$ (CNOT) transition is reduced by a potentially significant factor. This reduction is a consequence of the mixing between the states $|11\rangle$ and $|20\rangle$, which introduces a new term into the matrix element $\langle 3 | \frac{a_1}{2} \hat{\sigma}_x^{(1)} + \frac{a_2}{2} \hat{\sigma}_x^{(2)} | 2 \rangle$. For systems where both the anharmonicity and the coupling energy are small compared to the detuning between the qubits, the speed of the gate will be greatly suppressed. So in order to achieve large gate speeds with weakly anharmonic qubits, one must design the system with one or both of these two factors relatively large.

Next we analyse the leakage to the states outside the computational basis. The largest leakage arises from the transitions $|1\rangle \rightarrow |4\rangle$ and $|3\rangle \rightarrow |6\rangle$, because qubit 1 (the control qubit) is driven the strongest. The corresponding matrix elements and energy detunings are given by

$$\langle 4 | \frac{a_1}{2} \hat{\sigma}_x^{(1)} + \frac{a_2}{2} \hat{\sigma}_x^{(2)} | 1 \rangle \approx a_1 \frac{J}{\Delta_1 - \Delta_2} \frac{1}{\sqrt{2}} \left(-\frac{\delta_2}{(\Delta_1 - \Delta_2)} + \frac{J^2}{(\Delta_1 - \Delta_2)^2} \right), \quad (30a)$$

$$\langle 6 | \frac{a_1}{2} \hat{\sigma}_x^{(1)} + \frac{a_2}{2} \hat{\sigma}_x^{(2)} | 3 \rangle \approx a_1 \frac{J}{\Delta_1 - \Delta_2} \left(1 + \frac{\sqrt{2}}{4} \right), \quad (30b)$$

and

$$(E_4 - E_1) - (E_1 - E_0) \approx \delta_2 - \frac{2J^2\delta_2}{(\Delta_1 - \Delta_2)^2} \quad (31a)$$

$$(E_6 - E_3) - (E_3 - E_2) = \delta_2 - \frac{3J^2}{\Delta_1 - \Delta_2}. \quad (31b)$$

To avoid leakage, the transition strengths of the unwanted transitions should be lower (possibly much lower) than the detuning with the driving fields (similarly to section 2.1): $\langle l | \tilde{H}_{\text{drive}} | k \rangle < |\hbar\omega - \hbar\omega_{l \leftrightarrow k}|$. Both leakage transitions have approximately equal energy splitting ($\approx \delta_2$). The $|3\rangle \leftrightarrow |6\rangle$ transition clearly has the highest transition strength. Using this transition, we find the estimate for the maximum allowed Rabi frequency of the CNOT transition:

$$\omega_{R,\text{max}} = \frac{\delta_2}{2 + \sqrt{2}/2} \left[\frac{\delta_1}{(\Delta_1 - \Delta_2)} + \frac{J^2}{(\Delta_1 - \Delta_2)^2} \right]. \quad (32)$$

How close one can get to this estimated maximum is simulated numerically, and will be discussed soon.

A third issue that one needs to keep in mind when dealing with weakly anharmonic qubits is that the additional energy levels cause frequency shifts that break the symmetry $E_3 - E_2 = E_1 - E_0$. In particular, the energies of state 4 ($\approx |02\rangle$) and state 5 ($\approx |20\rangle$) will be close to the energy of state 3 ($\approx |11\rangle$). Fortunately, they cause shifts in opposite directions and almost cancel. The net shift is given by (see the expressions for the energies above)

$$\delta E_3 = \frac{2J^2}{\Delta_1 - \Delta_2 - \delta_2} - \frac{2J^2}{\Delta_1 - \Delta_2 + \delta_1} \approx \frac{2J^2(\delta_1 + \delta_2)}{(\Delta_1 - \Delta_2)^2}. \quad (33)$$

This frequency shift is not specific to the SD method, but is typical of weakly anharmonic qubits, and it results in an always-on interaction that drives a CPHASE gate.

We again perform numerical simulations to determine the total fidelity of all the combined errors. First we start with simulations where we vary the anharmonicity in order to see its effect on the gate speed and fidelity. We use three different combinations of anharmonicity: $(\delta_1/h = -400 \text{ MHz}, \delta_2/h = -360 \text{ MHz})$, $(\delta_1/h = -200 \text{ MHz}, \delta_2/h = -180 \text{ MHz})$ and $(\delta_1/h = -100 \text{ MHz}, \delta_2/h = -90 \text{ MHz})$. The other qubit parameters are $\Delta_1/h = 6 \text{ GHz}$, $\Delta_2/h = 5 \text{ GHz}$ and $J/h = 25 \text{ MHz}$.

The results are shown in figure 4. At low driving strength, the gate speeds have good correspondence with the expected dependence from the transition strength (equation (28b)), confirming the slowdown of the SD-CNOT gate for decreasing anharmonicity. This implies that for weakly anharmonic qubits it is recommended to design the detuning between the qubits to

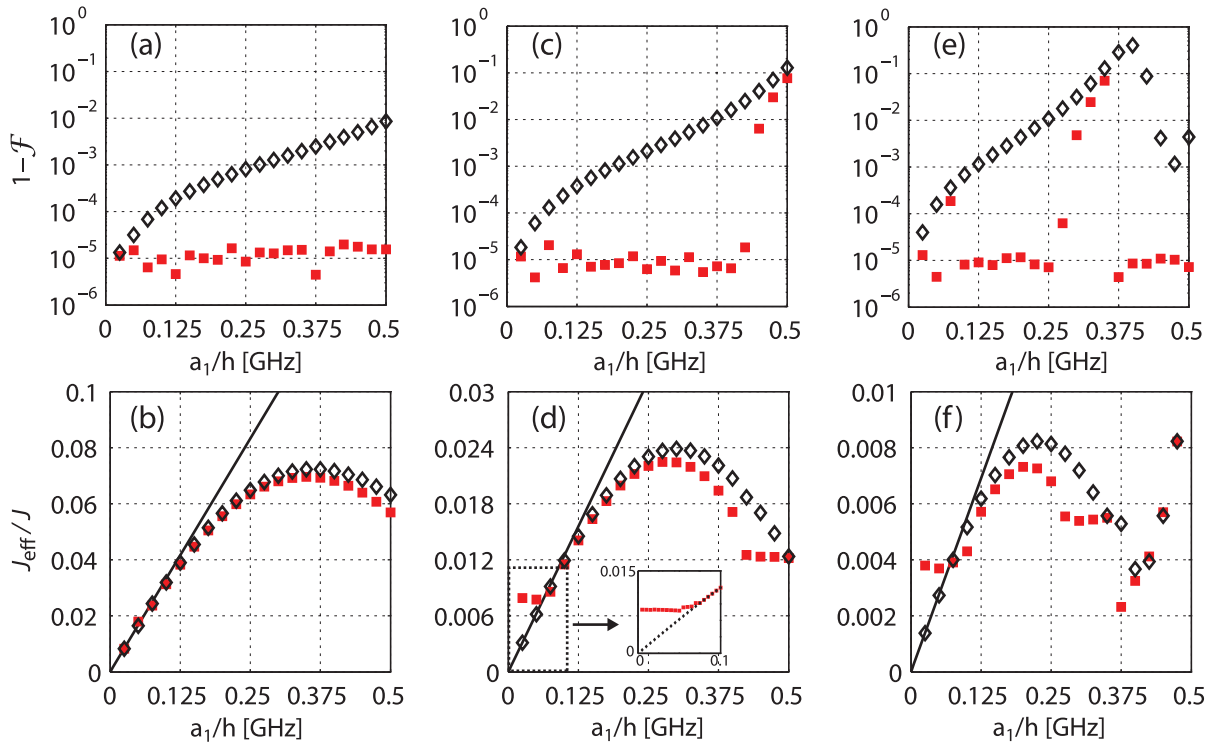


Figure 4. Numerical simulation of an SD-CNOT gate for three-level qubits with weak anharmonicity. Black diamonds represent the SD-CNOT gate including single-qubit phase gate corrections and the red squares represent the SD-CNOT gate including arbitrary single-qubit gates. Panels (a), (b) are calculated for anharmonicities of $\delta_1/h = -400$ MHz, $\delta_2/h = -360$ MHz, (c), (d) for $\delta_1/h = -200$ MHz, $\delta_2/h = -180$ MHz and (e), (f) for $\delta_1/h = -100$ MHz, $\delta_2/h = -90$ MHz. In panels (a), (c), (e) the gate error $1 - \mathcal{F}$ is plotted against the driving strength a_1 . Panels (b), (d), (f) give the corresponding gate speed J_{eff}/J for which fidelity is achieved. Dashed lines indicate the expected dependence from equation (28b). The qubit parameters used are $\Delta_1/h = 6$ GHz, $\Delta_2/h = 5$ GHz and $J/h = 25$ MHz.

be relatively small, so the negative impact on the gate speed due to weak anharmonicity can be minimized. Due to the low gate speeds, all the energy shifts induced by the driving and the higher-lying levels are also more significant. For this reason, the simple analytical calculation of the ac-Stark and Bloch–Siegert shifts of the control qubit (as was used for the calculation of the data represented by the blue circles in figure 3) no longer gives useful results. Therefore we do not plot the corresponding results in figure 4.

Another prominent feature is the decrease of the gate speed at high driving amplitudes. One possible explanation for this effect is a competition between the SD-CNOT gate and an ac-Stark-induced CPHASE gate. For figure 4(d) a plateau is observed at low driving strength. This plateau is related to the CPHASE evolution caused by level shifts induced by the higher energy levels of the qubits, and is therefore independent of the driving amplitude. As mentioned before, a CPHASE-type error can be corrected by altering the duration of the two-qubit driving and using single-qubit rotations. The plateau indicates that the CPHASE contribution to the final

CNOT gate even dominates over the SD contribution. The origin of the plateaus in panels (d) and (f) at high driving power is not known. The same holds for the sharp sudden increase in error. Note, however, that at these points the driving strength is already higher than would be advisable given the anharmonicity of the qubits.

A common approach to improving the gate speed and fidelity for weakly anharmonic qubits is to use pulse shaping (see, for example, the DRAG method [58, 59]). This approach could lead to improved gate speed and fidelity, but will not be discussed here.

In the experiment described in [41], a CR gate is performed. Given the close relationship between the SD and CR methods, we calculate, for comparison, the SD performance for the described system. The qubit parameters in this case are $\Delta_1/h = 5.854$ GHz, $\Delta_2/h = 5.528$ GHz, $\delta_1/h = 225$ MHz, $\delta_2/h = 255$ MHz and $J/h = 6$ MHz. The coupling J is estimated from the values provided in [41]. Figure 5 shows the result of the simulations. The gate speed in the simulations is in good agreement with the typical gate speeds in the experiment. With these system parameters one achieves a relatively high effective coupling, primarily thanks to the small detuning between the qubits. At very low driving strength we see a similar plateau as that in the previous parameter set and attribute this again to the level shifts due to the states outside the computational basis. From the fidelity data in figure 5(a), we conclude that the leakage to these states is negligible at these driving strengths: if there were significant leakage to these levels, the results obtained using the arbitrary single-qubit corrections, represented by red squares, could not lead to the gate improvement observed, because the single-qubit corrections we apply in the calculations cannot transfer back any state population that is lost during the SD gate. The increase of gate error for the results with arbitrary single-qubit gate corrections at $a_1/h = 0.1$ GHz has not yet been understood. Also we do not see significant slowdown of the gate at high driving strength as was measured in the experiment. A possible explanation for this is that different pulse shapes were used, that in the experiment DRAG-type [58, 59] pulses were also applied or that the presence of the resonator has an additional influence that is not covered by our direct coupling model. Nevertheless, the calculation illustrates that a similar performance can be expected for both the SD and CR methods.

7. Scalability

Let us now consider the scalability of the SD-CNOT gate to systems of more than two qubits. We take a system composed of a one-dimensional (1D) chain of N transversely coupled qubits and use the Jordan–Wigner transformation to turn it into a system of fermions occupying a 1D lattice with N sites. The transformation is given by

$$\hat{\sigma}_+^{(i)} = \prod_{j<i} (1 - 2\hat{c}_j^\dagger \hat{c}_j) \hat{c}_i, \quad (34a)$$

$$\hat{\sigma}_-^{(i)} = \prod_{j<i} (1 - 2\hat{c}_j^\dagger \hat{c}_j) \hat{c}_i^\dagger, \quad (34b)$$

$$\hat{\sigma}_z^{(i)} = 1 - 2\hat{c}_i^\dagger \hat{c}_i, \quad (34c)$$

where \hat{c} and \hat{c}^\dagger are annihilation and creation operators,

$$\hat{\sigma}_+ = \begin{pmatrix} 0 & 1 \\ 0 & 0 \end{pmatrix}, \quad \hat{\sigma}_- = \begin{pmatrix} 0 & 0 \\ 1 & 0 \end{pmatrix}, \quad (35)$$

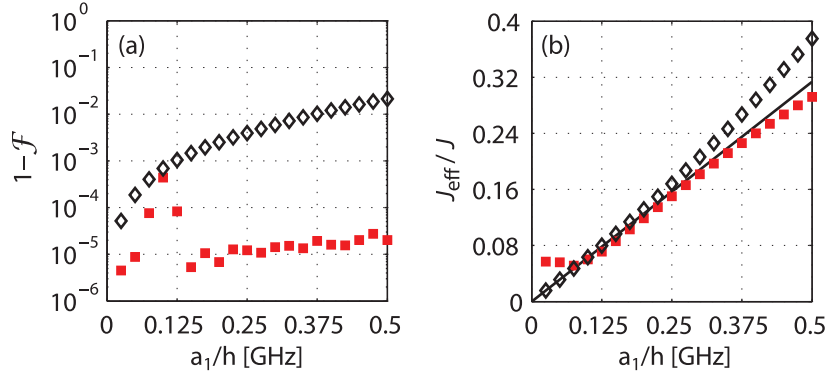


Figure 5. Numerical simulation of an SD-CNOT gate for three-level qubits with parameters similar to these of the experiment in [41]. The qubit parameters used are $\Delta_1/h = 5.854$ GHz, $\Delta_2/h = 5.528$ GHz, $\delta_1/h = 225$ MHz, $\delta_2/h = 255$ MHz and $J/h = 6$ MHz. Black diamonds represent the SD-CNOT gate including single-qubit phase gate corrections and the red squares represent the SD-CNOT gate including arbitrary single-qubit gates. In panel (a) the gate error $1 - \mathcal{F}$ is plotted against the driving strength a_1 . Panel (b) gives the corresponding gate speed J_{eff}/J for which fidelity is achieved. The black line indicates the expected dependence from equation (28b).

and $\hat{\sigma}_{x,z,+,-}^{(i)} = \mathbb{1}^{[1]} \otimes \mathbb{1}^{[2]} \dots \otimes \hat{\sigma}_{x,z,+,-}^{[i]} \dots \otimes \mathbb{1}^{[N]}$. This transformation transforms our original Hamiltonian, i.e.

$$\hat{H} = \sum_{i=1}^N -\frac{\Delta_i}{2} \hat{\sigma}_z^{(i)} + \sum_{i=1}^{N-1} J_{i,i+1} \hat{\sigma}_x^{(i)} \hat{\sigma}_x^{(i+1)}, \quad (36)$$

into

$$\hat{H} = \sum_{i=1}^N \Delta_i \hat{c}_i^\dagger \hat{c}_i + \sum_{i=1}^{N-1} J_{i,i+1} (\hat{c}_i^\dagger \hat{c}_{i+1} + \hat{c}_{i+1}^\dagger \hat{c}_i + \hat{c}_i^\dagger \hat{c}_{i+1}^\dagger + \hat{c}_{i+1} \hat{c}_i) + \text{const.} \quad (37)$$

This Hamiltonian does not look much simpler than the original one. In order to obtain something simple out of it, we now write the Hamiltonian as

$$\hat{H} = (\hat{c}_1^\dagger, \dots, \hat{c}_N^\dagger, \hat{c}_1, \dots, \hat{c}_N) M (\hat{c}_1, \dots, \hat{c}_N, \hat{c}_1^\dagger, \dots, \hat{c}_N^\dagger)^{\text{transpose}} + \text{const.}, \quad (38)$$

where M is a $2N \times 2N$ matrix. It is always possible to define new operators $\hat{\gamma}_i$ (with $i = 1, 2, \dots, N$) that also obey Fermi statistics and for which the Hamiltonian takes the simple form

$$\hat{H} = (\hat{\gamma}_1^\dagger, \dots, \hat{\gamma}_N^\dagger, \hat{\gamma}_1, \dots, \hat{\gamma}_N) \tilde{M} (\hat{\gamma}_1, \dots, \hat{\gamma}_N, \hat{\gamma}_1^\dagger, \dots, \hat{\gamma}_N^\dagger)^{\text{transpose}} + \text{const.}, \quad (39)$$

with a diagonal matrix \tilde{M} (note that this step can be carried out by diagonalizing the matrix M). In other words,

$$\hat{H} = \sum_{i=1}^N E_i \hat{\gamma}_i^\dagger \hat{\gamma}_i + \text{const.} \quad (40)$$

The physical meaning of the above Hamiltonian is the following. We have defined new creation and annihilation operators, which are combinations of the creation and annihilation operators for the original fermions. With the new definition, the Hamiltonian has turned into a Hamiltonian of non-interacting fermions. By diagonalizing the matrix M , we therefore obtain the available single-particle energy levels for these newly defined particles. This transformation can be interpreted as going from a description using the bare qubit states to a picture where the states are dressed by the qubit–qubit coupling energies. For a system with fixed qubit–qubit couplings, the dressed states are the most natural and physically relevant states to describe the dynamics [60].

The total energy of the entire system is obtained by identifying which single-particle energy levels are occupied and taking the sum of the energies of these levels. In other words, any energy eigenstate can be expressed as $\hat{\gamma}_i^\dagger \hat{\gamma}_j^\dagger \cdots \hat{\gamma}_k^\dagger |G\rangle$, where i, j, \dots, k denote the occupied single-particle states and $|G\rangle$ is the ground state of the system. This derivation provides a somewhat intuitive explanation to the result of [61], namely that the Larmor frequency of a given qubit is independent of the states of the other qubits. Since the original Hamiltonian is equivalent to a Hamiltonian that describes non-interacting fermions, it is natural that the change in energy induced by the addition of one particle into a certain energy level is independent of whether the other energy levels are occupied or not. This statement is independent of the strength of the coupling: even for strong coupling, where the energy eigenstates of the spin system are very involved (which corresponds to the fermion energy eigenstates having a large extension in space), the symmetric energy-level structure is still preserved. The only requirement is a 1D chain with a Hamiltonian of the form given in equation (36).

Now let us turn to the eigenstates of the Hamiltonian. In general, determining these eigenstates is harder than determining the eigenvalues, because even the ground state has a complicated form. The ground state $|G\rangle$ is defined by the set of conditions

$$\hat{\gamma}_i |G\rangle = 0 \quad (41)$$

for all values of i . In other words, there are no $\hat{\gamma}$ fermions in the ground state. However, in the language of the \hat{c} fermions, the above set of equations are not transparent at all and do not have any simple solution in general. This difficulty could make calculations complicated. However, we are mostly interested in the practical situation where the typical scale of the coupling energies (J) is small compared to the typical energy scale of the difference between different qubit splittings ($\delta\Delta$). We can therefore perform perturbation-theory calculations where we start by considering the case $J = 0$ first and then analyse the effect of adding a small coupling term.

In the case of zero coupling ($J = 0$), the matrix M is already diagonal, which means that the $\hat{\gamma}$ fermions coincide with the \hat{c} fermions. This means that each (single-particle) energy level is localized at one lattice site with no tunnelling between these sites. The state of the entire system is defined simply by specifying the occupation (0 or 1) of the different lattice sites. We now add a small coupling term ($J \neq 0$). For simplicity, we first consider the condition that the coupling strength is very small compared to the qubit Larmor frequencies ($J \ll \Delta$; note that here we use Δ , not $\delta\Delta$) and make a rotating wave approximation, meaning that the terms in equation (37) that create or annihilate two \hat{c} fermions are ignored:

$$\hat{H} \approx \sum_{i=1}^N \Delta_i \hat{c}_i^\dagger \hat{c}_i + \sum_{i=1}^{N-1} J_{i,i+1} (\hat{c}_i^\dagger \hat{c}_{i+1} + \hat{c}_{i+1}^\dagger \hat{c}_i) + \text{const.} \quad (42)$$

This approximation leads to a conceptual simplification, because we now know that creating a $\hat{\gamma}$ fermion in a given energy level corresponds to creating a \hat{c} fermion in a quantum state that is (in general) spread over the entire lattice, with no involved mixing between creation and annihilation operators. Another important result of the above approximation is that the ground state reduces to a very simple form. Regardless of the exact form of the operators $\hat{\gamma}_i$ in terms of the operators \hat{c}_i , the set of conditions $\hat{\gamma}_i |G\rangle = 0$ leads to the set of conditions $\hat{c}_i |G\rangle = 0$, such that the ground state corresponds to zero occupation of all the single-particle states in both languages. Note that the number of particles is also the same for any state in both languages ($\sum \hat{c}^\dagger \hat{c} = \sum \hat{\gamma}^\dagger \hat{\gamma}$).

With the above approximation, we have turned the Hamiltonian into a Hamiltonian that conserves the number of particles (even in the language of the \hat{c} operators). Note also that there are no interaction terms in the Hamiltonian. We can therefore proceed to calculate the form of the operators $\hat{\gamma}_i$ by considering a single-particle problem. (This is allowed because in the absence of interactions the form of the different single-particle wave functions will be insensitive to whether other wave functions are occupied or not.) For this purpose we imagine that there is only one particle in the system, and this particle can hop (i.e. tunnel) between the different lattice sites.

When calculating the form of the single-particle wave functions, we use the condition $J \ll \delta\Delta$. This condition implies that although the \hat{c} fermions can hop between different lattice sites, the hopping matrix elements are small compared to the detuning between neighbouring sites. As a result, the different single-particle states (i.e. those described by the $\hat{\gamma}$ fermions) will each be concentrated around one lattice site (recall that when $J = 0$ the states are completely localized at individual lattice sites). One can calculate the spread of the states using perturbation theory. Writing

$$\hat{\gamma}_i = \sum_{j=1}^N \psi_i(j) \hat{c}_j, \quad (43)$$

we find that

$$\begin{aligned} \psi_i(i) &= 1 + O\left(\frac{J}{\delta\Delta}\right)^2, \\ \psi_i(i \pm 1) &= \frac{J_{i,i\pm 1}}{\Delta_i - \Delta_{i\pm 1}} + O\left(\frac{J}{\delta\Delta}\right)^3, \\ \psi_i(i \pm 2) &= \frac{J_{i,i\pm 1} J_{i\pm 1,i\pm 2}}{(\Delta_i - \Delta_{i\pm 1})(\Delta_{i\pm 1} - \Delta_{i\pm 2})} + O\left(\frac{J}{\delta\Delta}\right)^4, \\ &\vdots \\ \psi_i(j) &\sim \left(\frac{J}{\delta\Delta}\right)^{|i-j|} \quad \text{when } |i-j| \gg 1. \\ &\vdots \end{aligned} \quad (44)$$

Note that the above relation can be inverted straightforwardly:

$$\hat{c}_i = \sum_{j=1}^N \psi_j(i) \hat{\gamma}_j. \quad (45)$$

In principle, the localization situation changes when two or more lattice sites are degenerate. For example, in the case of twofold degeneracy and an otherwise symmetric environment, the (single-particle) energy eigenstates will be symmetric and antisymmetric superpositions of the particle being at one of the two sites. However, provided that these degeneracies occur only for largely separated lattice sites, the effective tunnelling matrix element will be exponentially small at the distance between the two sites in question: (assuming $j > i$)

$$J_{ij,\text{effective}} \sim \frac{J_{i,i+1}}{\Delta_i - \Delta_{i+1}} \times \frac{J_{i+1,i+2}}{\Delta_i - \Delta_{i+2}} \times \cdots \times \frac{J_{j-2,j-1}}{\Delta_i - \Delta_{j-1}} \times J_{j-1,j}. \quad (46)$$

We can therefore ignore such long-range tunnelling and focus on the practically relevant case when the $\hat{\gamma}$ fermions and the \hat{c} fermions are almost equal, with exponentially decaying tails describing the spread of the $\hat{\gamma}$ fermions. This situation is related to the phenomenon of Anderson localization, where disorder causes the single-particle states to be localized with exponentially decaying tails.

We can now start performing the calculations for the Rabi frequencies. Before going into long expressions, we make the following observation. If a driving signal is applied to qubit i , the driving term in the Hamiltonian can be expressed in the language of fermions as

$$\hat{H}_{\text{drive}} = \prod_{j < i} (1 - 2\hat{c}_j^\dagger \hat{c}_j) (\hat{c}_i + \hat{c}_i^\dagger) \cos(\omega t). \quad (47)$$

The relevant matrix elements for the purposes of evaluating the Rabi frequency of qubit k therefore have the form

$$\langle 0 | \hat{\gamma}_m \hat{\gamma}_n \cdots \hat{\gamma}_p \left[\hat{\gamma}_k \prod_{j < i} (1 - 2\hat{c}_j^\dagger \hat{c}_j) (\hat{c}_i + \hat{c}_i^\dagger) \right] \hat{\gamma}_p^\dagger \cdots \hat{\gamma}_n^\dagger \hat{\gamma}_m^\dagger | 0 \rangle, \quad (48)$$

where the index i represents the driven qubit and the operators on the far right and far left (i.e. those with indices m, n, \dots, p) describe the state of the surrounding qubits. Let us now assume that i and m are separated by a large distance. From the above localization argument, we know that the fermion created by the operator $\hat{\gamma}_m^\dagger$ is concentrated mostly on one side of site i (i.e. to the right if $m > i$ and to the left if $m < i$), with only a very small probability of occupying site i or crossing to the opposite side. As mentioned above, this probability decreases exponentially with the distance between i and m . We can therefore make the approximation that the operators $(\hat{c}_i + \hat{c}_i^\dagger)$ and $\hat{\gamma}_m^\dagger$ anti-commute and that the operators $\prod_{j < i} (1 - 2\hat{c}_j^\dagger \hat{c}_j)$ and $\hat{\gamma}_m^\dagger$ either commute or anti-commute, depending on whether $m > i$ or $m < i$. Note that here the operator $\prod_{j < i} (1 - 2\hat{c}_j^\dagger \hat{c}_j)$ counts the number of particles to the left of site i and produces a sign factor ± 1 depending on that number. This approximation, along with the anti-commutation relations between the different $\hat{\gamma}$ operators, allow us to move the operator $\hat{\gamma}_m^\dagger$ from the far right of the above expression to just right of the operator $\hat{\gamma}_m$, with only a minus sign appearing whenever $m < i$. The combination $\hat{\gamma}_m \hat{\gamma}_m^\dagger$ applied to $\langle 0 |$ does not affect the state, and these two operators can be ignored. We conclude therefore that the effect of occupation of a distant single-particle state is exponentially small and can be ignored. We now have to decide where to draw the line between the states we will consider and the states we will ignore. Since we are interested in the lowest-order corrections, we shall consider only the effect of the nearest-neighbour states, which will produce the lowest-order corrections.

As a first step, let us consider the Rabi frequency of qubit i when driving only that qubit. Since under our approximation we consider only the effect of occupation of the two

neighbouring sites, we only need to consider a three-qubit system (the algebra can be easily generalized to longer chains). It is straightforward to show that for driving qubit 1, we have

$$\begin{aligned}\langle 0|\hat{\gamma}_1(\hat{c}_1 + \hat{c}_1^\dagger)|0\rangle &= \langle 0|\hat{\gamma}_2\hat{\gamma}_1(\hat{c}_1 + \hat{c}_1^\dagger)\hat{\gamma}_2^\dagger|0\rangle = \langle 0|\hat{\gamma}_3\hat{\gamma}_1(\hat{c}_1 + \hat{c}_1^\dagger)\hat{\gamma}_3^\dagger|0\rangle \\ &= \langle 0|\hat{\gamma}_2\hat{\gamma}_3\hat{\gamma}_1(\hat{c}_1 + \hat{c}_1^\dagger)\hat{\gamma}_3^\dagger\hat{\gamma}_2^\dagger|0\rangle = \psi_1(1),\end{aligned}\quad (49)$$

and a similar relation applies to driving qubit 3. For driving qubit 2 we have

$$\langle 0|\hat{\gamma}_2(1 - 2\hat{c}_1^\dagger\hat{c}_1)(\hat{c}_2 + \hat{c}_2^\dagger)|0\rangle = \psi_2(2),\quad (50a)$$

$$-\langle 0|\hat{\gamma}_1\hat{\gamma}_2(1 - 2\hat{c}_1^\dagger\hat{c}_1)(\hat{c}_2 + \hat{c}_2^\dagger)\hat{\gamma}_1^\dagger|0\rangle \approx \psi_2(2) \left[1 + \frac{2J_{12}^2 J_{23}^2}{(\Delta_1 - \Delta_2)(\Delta_2 - \Delta_3)(\Delta_1 - \Delta_3)^2} \right],\quad (50b)$$

$$\langle 0|\hat{\gamma}_3\hat{\gamma}_2(1 - 2\hat{c}_1^\dagger\hat{c}_1)(\hat{c}_2 + \hat{c}_2^\dagger)\hat{\gamma}_3^\dagger|0\rangle \approx \psi_2(2) \left[1 + \frac{2J_{12}^2 J_{23}^2}{(\Delta_1 - \Delta_2)(\Delta_2 - \Delta_3)(\Delta_1 - \Delta_3)^2} \right],\quad (50c)$$

$$-\langle 0|\hat{\gamma}_1\hat{\gamma}_3\hat{\gamma}_2(1 - 2\hat{c}_1^\dagger\hat{c}_1)(\hat{c}_2 + \hat{c}_2^\dagger)\hat{\gamma}_3^\dagger\hat{\gamma}_1^\dagger|0\rangle = \psi_2(2).\quad (50d)$$

Therefore the Rabi frequencies of qubits 1 and 3 (which are at the end of the chain) do not depend on the state of the other qubits (this result holds even for longer chains and can be shown rigorously using Wick's theorem), while the Rabi frequency of qubit 2 shows some dependence on the states of the surrounding qubits, with a spread that is of the order of $(J/\delta\Delta)^4$. These results agree with the numerically derived results of [61].

We now turn to the Rabi frequencies when driving two qubits simultaneously in order to implement the SD-CNOT gate. We now have driving terms applied to two qubits. As a result, in addition to the expressions calculated above, we need to evaluate expressions of the form

$$\langle 0|\hat{\gamma}_m\hat{\gamma}_n \cdots \hat{\gamma}_p \left[\hat{\gamma}_i \prod_{j \leq i} (1 - 2\hat{c}_j^\dagger\hat{c}_j)(\hat{c}_{i+1} + \hat{c}_{i+1}^\dagger) \right] \hat{\gamma}_p^\dagger \cdots \hat{\gamma}_n^\dagger\hat{\gamma}_m^\dagger|0\rangle.\quad (51)$$

As above, we ignore all the distant qubits. We consider a four-qubit chain with the driving applied to qubit 3 such that qubit 2 changes its state (i.e. $i = 2$ in equation (51)). Here we take a chain of length four, to incorporate also the influence of the nearest neighbour of the driven qubit. The relevant matrix elements are given by

$$\langle 0|\hat{\gamma}_2 \prod_{j \leq 2} (1 - 2\hat{c}_j^\dagger\hat{c}_j)(\hat{c}_3 + \hat{c}_3^\dagger)|0\rangle = \psi_2(3),\quad (52a)$$

$$\begin{aligned}-\langle 0|\hat{\gamma}_1\hat{\gamma}_2 \prod_{j \leq 2} (1 - 2\hat{c}_j^\dagger\hat{c}_j)(\hat{c}_3 + \hat{c}_3^\dagger)\hat{\gamma}_1^\dagger|0\rangle &= \psi_2(3) + 2\psi_1(4) \\ &\times \frac{J_{12}J_{23}^2J_{34}}{(\Delta_1 - \Delta_3)(\Delta_2 - \Delta_3)(\Delta_2 - \Delta_4)(\Delta_1 - \Delta_4)},\end{aligned}\quad (52b)$$

$$\langle 0|\hat{\gamma}_4\hat{\gamma}_2 \prod_{j \leq 2} (1 - 2\hat{c}_j^\dagger\hat{c}_j)(\hat{c}_3 + \hat{c}_3^\dagger)\hat{\gamma}_4^\dagger|0\rangle \approx \psi_2(3) + 2\psi_4(2)\psi_4(3)\psi_2(2),\quad (52c)$$

$$-\langle 0 | \hat{\gamma}_1 \hat{\gamma}_4 \hat{\gamma}_2 \prod_{j \leq 2} (1 - 2\hat{c}_j^\dagger \hat{c}_j) (\hat{c}_3 + \hat{c}_3^\dagger) \hat{\gamma}_4^\dagger \hat{\gamma}_1^\dagger | 0 \rangle \approx \psi_2(3) + 2\psi_4(2)\psi_4(3)\psi_2(2), \quad (52d)$$

and similar expressions for the case when the operator $\hat{\gamma}_3$ appears, e.g.

$$-\langle 0 | \hat{\gamma}_1 \hat{\gamma}_3 \hat{\gamma}_4 \hat{\gamma}_2 \prod_{j \leq 2} (1 - 2\hat{c}_j^\dagger \hat{c}_j) (\hat{c}_3 + \hat{c}_3^\dagger) \hat{\gamma}_4^\dagger \hat{\gamma}_3^\dagger \hat{\gamma}_1^\dagger | 0 \rangle = \psi_2(3). \quad (53)$$

We therefore arrive at the main result of this section:

$$\langle 0 | \hat{\gamma}_2 \prod_{j \leq 2} (1 - 2\hat{c}_j^\dagger \hat{c}_j) (\hat{c}_3 + \hat{c}_3^\dagger) | 0 \rangle = \psi_2(3), \quad (54a)$$

$$-\langle 0 | \hat{\gamma}_1 \hat{\gamma}_2 \prod_{j \leq 2} (1 - 2\hat{c}_j^\dagger \hat{c}_j) (\hat{c}_3 + \hat{c}_3^\dagger) \hat{\gamma}_1^\dagger | 0 \rangle = \psi_2(3) \left(1 + O\left(\frac{J}{\delta\Delta}\right)^6 \right), \quad (54b)$$

$$\langle 0 | \hat{\gamma}_4 \hat{\gamma}_2 \prod_{j \leq 2} (1 - 2\hat{c}_j^\dagger \hat{c}_j) (\hat{c}_3 + \hat{c}_3^\dagger) \hat{\gamma}_4^\dagger | 0 \rangle = \psi_2(3) \left(1 + O\left(\frac{J}{\delta\Delta}\right)^2 \right), \quad (54c)$$

$$-\langle 0 | \hat{\gamma}_1 \hat{\gamma}_4 \hat{\gamma}_2 \prod_{j \leq 2} (1 - 2\hat{c}_j^\dagger \hat{c}_j) (\hat{c}_3 + \hat{c}_3^\dagger) \hat{\gamma}_4^\dagger \hat{\gamma}_1^\dagger | 0 \rangle = \psi_2(3) \left(1 + O\left(\frac{J}{\delta\Delta}\right)^2 \right), \quad (54d)$$

and similar expressions for the case when the operator $\hat{\gamma}_3$ appears.

The relative error in the CNOT gate will therefore be of the order of $(J/\delta\Delta)^2$. This result is in agreement with the numerical calculations in [61], where also a spread of $(J/\delta\Delta)^2$ is found in the matrix elements for flipping qubit i when driving qubit $i + 1$, depending on the states of the surrounding qubits.

The scaling of the error with $(J/\delta\Delta)^2$ is comparable to the other schemes for implementing entangling of two-qubit gates. The SD-CNOT gate has, however, the added advantage that the qubit level splittings need not be shifted. The shifting of energy levels gets increasingly complicated in multi-qubit systems, where the multitude of levels makes it harder to avoid crossing resonances that lead to unwanted evolution and entanglement. Also the freedom that the qubits do not have to be nearest neighbour in frequency can make the design of a multi-qubit system simpler.

8. Conclusion and discussion

We have theoretically analysed all the properties of the SD-CNOT gate that are important for its implementation in experiments. In the weak-driving limit and in the absence of decoherence, the fidelity of the gate is 100%. For increasing driving strength the fidelity of the gate decreases due to the off-resonant driving of other transitions in the system. The off-resonant driving can induce spurious excitation of these transitions and ac-Stark shifts of the levels, inducing an undesired single-qubit and (entangling) two-qubit evolution. We analysed the strength of these effects analytically, and in addition performed a full numerical simulation of the time evolution of the system. For the SD-CNOT gate without extra optimizations, the numerical simulations show a fidelity of 99% and 99.99% for gate speeds corresponding to $0.48J$ and $0.07J$, respectively. At

high gate speeds the fidelity can be boosted by employing single-qubit correction pulses before and after the two-qubit driving.

The gate performance was also analysed for multi-level qubits with weak anharmonicity of the energy splittings. As expected, it was found that the gate speed for a specified fidelity goes down for decreasing anharmonicity of the qubits. The energy shifts of the computational states due to the higher levels and leakage to these higher levels can both play an important role. We determined fidelities of 99% and 99.99% for gate speeds corresponding to 0.08δ and 0.02δ (for $\delta \approx 200$ MHz). The gate speed can be increased by designing a relatively large coupling strength or low detuning between the qubits, or both. Another possible route for increasing the gate speed and/or fidelity for weakly anharmonic qubits is by using pulse shaping of the driving field.

The scalability of the SD-CNOT gate was also studied. For a 1D array of qubits the error in the gate scales as $(J/\delta\Delta)^2$, which is comparable to the other schemes for implementing entangling two-qubit gates. The SD-CNOT gate has, however, the favourable properties that the qubit level splittings need not be shifted, and neither is it required that the qubits be nearest neighbour in frequency. These properties can make a significant difference to the design of multi-qubit systems. We conclude that, in terms of fidelity, gate speed and potential for scalability, the SD-CNOT gate is a valuable addition to the existing range of entangling gates.

Acknowledgments

We thank D Ristè for discussions. PCdG, CJPMH and JEM were supported by NanoNed and FOM and the EU projects EuroSQIP and CORNER. SA and FN were partially supported by ARO, NSF grant no. 0726909, JSPS-RFBR contract no. 12-02-92100, Grant-in-Aid for Scientific Research (S), MEXT Kakenhi on Quantum Cybernetics and the JSPS via its FIRST program. AL was supported by NSERC. LDC was partially funded by NWO.

Appendix A. Transformation to rotating frame

We start from the Hamiltonian and driving term as given by equations (1) and (3). For this calculation we use the energy eigenbasis in the absence of the driving term (i.e. the states $|0\rangle$, $|1\rangle$, $|2\rangle$ and $|3\rangle$ in equations (9)). The Hamiltonian without the driving term takes the form:

$$\hat{H}_0 = \frac{1}{2} \begin{pmatrix} -\sqrt{(\Delta_1 + \Delta_2)^2 + 4J^2} & 0 & 0 & 0 \\ 0 & -\sqrt{(\Delta_1 - \Delta_2)^2 + 4J^2} & 0 & 0 \\ 0 & 0 & \sqrt{(\Delta_1 - \Delta_2)^2 + 4J^2} & 0 \\ 0 & 0 & 0 & \sqrt{(\Delta_1 + \Delta_2)^2 + 4J^2} \end{pmatrix}, \quad (\text{A.1})$$

and the matrix elements of the driving term \hat{H}_{drive} (equation (3)) are given by

$$\begin{aligned} \langle 1 | \hat{H}_{\text{drive}} | 0 \rangle &= -a_1 \sin \theta_+ \cos(\omega t + \varphi_1) + a_2 \cos \theta_- \cos(\omega t + \varphi_2), \\ \langle 2 | \hat{H}_{\text{drive}} | 0 \rangle &= +a_1 \cos \theta_+ \cos(\omega t + \varphi_1) + a_2 \sin \theta_- \cos(\omega t + \varphi_2), \\ \langle 3 | \hat{H}_{\text{drive}} | 2 \rangle &= +a_1 \sin \theta_+ \cos(\omega t + \varphi_1) + a_2 \cos \theta_- \cos(\omega t + \varphi_2), \\ \langle 3 | \hat{H}_{\text{drive}} | 1 \rangle &= +a_1 \cos \theta_+ \cos(\omega t + \varphi_1) - a_2 \sin \theta_- \cos(\omega t + \varphi_2), \\ \langle i | \hat{H}_{\text{drive}} | j \rangle &= \langle j | \hat{H}_{\text{drive}} | i \rangle. \end{aligned} \quad (\text{A.2})$$

All other matrix elements vanish.

We now make a transformation to a convenient rotating frame. This means that instead of solving the Schrödinger equation for $|\psi\rangle$, we solve an equation for

$$|\tilde{\psi}\rangle = \hat{U}(t)|\psi\rangle, \quad (\text{A.3})$$

where

$$\hat{U}(t) = e^{iut/\hbar}, \quad u = \begin{pmatrix} -\hbar\omega & 0 & 0 & 0 \\ 0 & 0 & 0 & 0 \\ 0 & 0 & 0 & 0 \\ 0 & 0 & 0 & \hbar\omega \end{pmatrix}. \quad (\text{A.4})$$

Note that u is not the only possible choice that could serve our purpose here. Other transformations will lead to the same result.

The laboratory-frame state $|\psi\rangle$ satisfies the Schrödinger equation: $i\hbar \frac{d}{dt} |\psi\rangle = \hat{H} |\psi\rangle$. In the rotating frame, the state $|\tilde{\psi}\rangle$ should also satisfy the Schrödinger equation: $i\hbar \frac{d}{dt} |\tilde{\psi}\rangle = \tilde{H} |\tilde{\psi}\rangle$. From these equations the transformation is easily derived:

$$\begin{aligned} \tilde{H} &= \hat{U} \hat{H} \hat{U}^\dagger - i\hbar \hat{U} \frac{d\hat{U}^\dagger}{dt} \\ &= \hat{U} \hat{H} \hat{U}^\dagger - u. \end{aligned} \quad (\text{A.5})$$

With the total Hamiltonian given by $\hat{H} = \hat{H}_0 + \hat{H}_{\text{drive}}$, this results in

$$\begin{aligned} \tilde{H}_0 &= \hat{U} \hat{H}_0 \hat{U}^\dagger - u \\ &= \hat{H}_0 - u \\ &= \begin{pmatrix} -\frac{\sqrt{(\Delta_1+\Delta_2)^2+4J^2}}{2} + \hbar\omega & 0 & 0 & 0 \\ 0 & -\frac{\sqrt{(\Delta_1-\Delta_2)^2+4J^2}}{2} & 0 & 0 \\ 0 & 0 & \frac{\sqrt{(\Delta_1-\Delta_2)^2+4J^2}}{2} & 0 \\ 0 & 0 & 0 & \frac{\sqrt{(\Delta_1+\Delta_2)^2+4J^2}}{2} - \hbar\omega \end{pmatrix}, \end{aligned} \quad (\text{A.6a})$$

$$\tilde{H}_{\text{drive}} = \hat{U} \hat{H}_{\text{drive}} \hat{U}^\dagger. \quad (\text{A.6b})$$

The matrix elements of \tilde{H}_{drive} can conveniently be split into $\tilde{H}_{\text{drive}} = \tilde{V} + \tilde{W}$, where \tilde{V} contains the time-independent and \tilde{W} the time-dependent terms:

$$\begin{aligned} \langle 1|\tilde{V}|0\rangle &= e^{i\omega t} \langle 1|\hat{V}|0\rangle \\ &= \frac{1}{2} (-a_1 \sin \theta_+ e^{-i\varphi_1} + a_2 \cos \theta_- e^{-i\varphi_2}), \\ \langle 2|\tilde{V}|0\rangle &= \frac{1}{2} (+a_1 \cos \theta_+ e^{-i\varphi_1} + a_2 \sin \theta_- e^{-i\varphi_2}), \\ \langle 3|\tilde{V}|2\rangle &= \frac{1}{2} (+a_1 \sin \theta_+ e^{-i\varphi_1} + a_2 \cos \theta_- e^{-i\varphi_2}), \\ \langle 3|\tilde{V}|1\rangle &= \frac{1}{2} (+a_1 \cos \theta_+ e^{-i\varphi_1} - a_2 \sin \theta_- e^{-i\varphi_2}), \\ \langle i|\tilde{V}|j\rangle &= \langle j|\tilde{V}|i\rangle^*, \\ \langle 1|\tilde{W}|0\rangle &= \frac{1}{2} (-a_1 \sin \theta_+ e^{i\varphi_1} + a_2 \cos \theta_- e^{i\varphi_2}) e^{i2\omega t}, \\ \langle 2|\tilde{W}|0\rangle &= \frac{1}{2} (+a_1 \cos \theta_+ e^{i\varphi_1} + a_2 \sin \theta_- e^{i\varphi_2}) e^{i2\omega t}, \end{aligned} \quad (\text{A.7})$$

$$\begin{aligned}\langle 3|\tilde{W}|2\rangle &= \frac{1}{2} (+a_1 \sin \theta_+ e^{i\varphi_1} + a_2 \cos \theta_- e^{i\varphi_2}) e^{i2\omega t}, \\ \langle 3|\tilde{W}|1\rangle &= \frac{1}{2} (+a_1 \cos \theta_+ e^{i\varphi_1} - a_2 \sin \theta_- e^{i\varphi_2}) e^{i2\omega t}, \\ \langle i|\tilde{W}|j\rangle &= \langle j|\tilde{W}|i\rangle^*.\end{aligned}$$

Transforming back to the laboratory-frame, the matrix elements in the energy eigenbasis of \hat{V} and \hat{W} are given by

$$\begin{aligned}\langle 1|\hat{V}|0\rangle &= \frac{1}{2} (-a_1 \sin \theta_+ e^{-i\varphi_1} + a_2 \cos \theta_- e^{-i\varphi_2}) e^{-i\omega t}, \\ \langle 2|\hat{V}|0\rangle &= \frac{1}{2} (+a_1 \cos \theta_+ e^{-i\varphi_1} + a_2 \sin \theta_- e^{-i\varphi_2}) e^{-i\omega t}, \\ \langle 3|\hat{V}|2\rangle &= \frac{1}{2} (+a_1 \sin \theta_+ e^{-i\varphi_1} + a_2 \cos \theta_- e^{-i\varphi_2}) e^{-i\omega t}, \\ \langle 3|\hat{V}|1\rangle &= \frac{1}{2} (+a_1 \cos \theta_+ e^{-i\varphi_1} - a_2 \sin \theta_- e^{-i\varphi_2}) e^{-i\omega t}, \\ \langle i|\hat{V}|j\rangle &= \langle j|\hat{V}|i\rangle^*, \\ \langle i|\hat{W}|j\rangle &= \langle i|\hat{V}|j\rangle^*.\end{aligned}\tag{A.8}$$

From these equations we see that \hat{V} describes the co-rotating and \hat{W} the counter-rotating field with respect to the Larmor precession of the system.

The representation of \hat{V} in the uncoupled-qubit basis can be straightforwardly calculated from the result of equation (A.8), however, the result is a rather involved and large matrix. The main results of this appendix, i.e. the matrix elements in equation (A.7), can be reproduced exactly by use of the terms $\tilde{H}_{\text{drive}}^+$ and $\tilde{H}_{\text{drive}}^-$ as described in section 2.1. This approach is valid for the purpose of calculating transition strengths, but for other purposes it can be necessary to use the full representation \hat{V} and \hat{W} .

Note that in the derivation in this appendix no approximations have been made: we have only performed transformations and rearranged equations.

Appendix B. Quantum mechanical description of the driving field

In the other sections, we have treated the driving field as a classical field. In this section, we provide a description of the driven system where the driving field is treated quantum mechanically. With this description we verify some of the results on level shifts and gate errors obtained using the classical field description. In addition the description provided here can be used as a starting point to further investigate the strong-driving regime, maximum gate speed and the related gate errors.

For this calculation, we use the dressed-state picture. We consider a model composed of two qubits and a harmonic oscillator containing a large number of photons. In this picture the Hamiltonian becomes time independent and the frequency of the driving field now appears as $\hbar\omega\hat{b}^\dagger\hat{b}$, where \hat{b} and \hat{b}^\dagger are the annihilation and creation operators of the quantized field. The driving term $a_i \cos(\omega t)$ in the original Hamiltonian (i.e. the Hamiltonian in which the driving field is treated as classical) is now replaced by the operator $g_i(\hat{b} + \hat{b}^\dagger)$, where g_i represents the coupling strength between the resonator and qubit i .

We take the case where qubit 2 is the target qubit and where the $|00\rangle \leftrightarrow |01\rangle$ transition is to be darkened. In this case $\varphi_1 = \varphi_2$. Again, for simplicity in the expressions, we take $\varphi_1 = \varphi_2 = 0$. Unlike in the weak-driving limit, we do not impose the relations $\hbar\omega = E_1 - E_0$

and $a_2/a_1 = \sin \theta_+ / \cos \theta_-$. Instead, we leave the coupling strengths between the oscillator and the two qubits as tunable parameters to be decided later.

Assuming that the qubit frequencies Δ_1 and Δ_2 are much larger than the coupling and driving frequency scales, the energy-level structure breaks up into blocks of four energy levels in each block, with negligible effects caused by the coupling between the different blocks. We therefore consider the spaces spanned by the states $|0, N+1\rangle$, $|1, N\rangle$, $|2, N\rangle$ and $|3, N-1\rangle$. In this space the Hamiltonian reads

$$\hat{H} = \begin{pmatrix} 0 & -C_1 \sin \theta_+ + C_2 \cos \theta_- & C_1 \cos \theta_+ + C_2 \sin \theta_- & 0 \\ -C_1 \sin \theta_+ + C_2 \cos \theta_- & (E_1 - E_0) - \hbar\omega & 0 & C_1 \cos \theta_+ - C_2 \sin \theta_- \\ C_1 \cos \theta_+ + C_2 \sin \theta_- & 0 & (E_2 - E_0) - \hbar\omega & C_1 \sin \theta_+ + C_2 \cos \theta_- \\ 0 & C_1 \cos \theta_+ - C_2 \sin \theta_- & C_1 \sin \theta_+ + C_2 \cos \theta_- & (E_1 + E_2 - 2E_0) - 2\hbar\omega \end{pmatrix}, \quad (\text{B.1})$$

where $C_i = \sqrt{N} g_i$, with N the number of photons in the resonator, and we have made the assumption that N is large, such that $N \approx N+1$.

One can now argue that the condition for a darkened transition is that the two corresponding energy levels must be degenerate: what corresponds to driven (Rabi) evolution in the previous picture can be regarded as Larmor precession in the current picture, and for Larmor precession to be suppressed the corresponding states have to be degenerate.

If we make the approximation that the driving amplitudes are small compared to the detuning, the above Hamiltonian can be approximated as

$$\hat{H}_0 \approx \begin{pmatrix} 0 & -C_1 \sin \theta_+ + C_2 \cos \theta_- & 0 & 0 \\ -C_1 \sin \theta_+ + C_2 \cos \theta_- & (E_1 - E_0) - \hbar\omega & 0 & 0 \\ 0 & 0 & (E_2 - E_0) - \hbar\omega & C_1 \sin \theta_+ + C_2 \cos \theta_- \\ 0 & 0 & C_1 \sin \theta_+ + C_2 \cos \theta_- & (E_1 + E_2 - 2E_0) - 2\hbar\omega \end{pmatrix}, \quad (\text{B.2})$$

and then it is obvious that the lowest two energy levels are degenerate for the choice of parameters $(E_1 - E_0) - \hbar\omega = 0$ and $-C_1 \sin \theta_+ + C_2 \cos \theta_- = 0$, which is actually a different way of writing the condition derived in the semiclassical derivation (equation (13)).

When we do not make the approximation of small driving amplitudes, using the full Hamiltonian in equation (B.1), the matrix elements H_{02} , H_{20} , H_{13} and H_{31} will mix all the quantum states to form the new, corrected energy eigenstates. If we think in terms of an order-by-order expansion of the effects of these matrix elements, we can see that the matrix elements H_{02} and H_{20} will cause mixing and repulsion between the states $|0, N+1\rangle$ and $|2, N\rangle$, while the matrix elements H_{13} and H_{31} will cause mixing and repulsion between the states $|1, N\rangle$ and $|3, N-1\rangle$. To first order, the corrected quantum states are:

$$|0, N+1\rangle' = |0, N+1\rangle - \frac{C_1 \cos \theta_+ + C_2 \sin \theta_-}{E_2 - E_0 - \hbar\omega} |2, N\rangle, \quad (\text{B.3a})$$

$$|1, N\rangle' = |1, N\rangle - \frac{C_1 \cos \theta_+ - C_2 \sin \theta_-}{E_2 - E_0 - \hbar\omega} |3, N-1\rangle, \quad (\text{B.3b})$$

$$|2, N\rangle' = |2, N\rangle + \frac{C_1 \cos \theta_+ + C_2 \sin \theta_-}{E_2 - E_0 - \hbar\omega} |0, N+1\rangle, \quad (\text{B.3c})$$

$$|3, N-1\rangle' = |3, N-1\rangle + \frac{C_1 \cos \theta_+ - C_2 \sin \theta_-}{E_2 - E_0 - \hbar\omega} |1, N\rangle, \quad (\text{B.3d})$$

and, to last order, the corrections to the energies ($\delta E_i = E_i' - E_i$) are given by

$$\delta E_0 = -\delta E_2 = -\frac{(C_1 \cos \theta_+ + C_2 \sin \theta_-)^2}{E_2 - E_0 - \hbar\omega}, \quad (\text{B.4a})$$

$$\delta E_1 = -\delta E_3 = -\frac{(C_1 \cos \theta_+ - C_2 \sin \theta_-)^2}{E_2 - E_0 - \hbar\omega}. \quad (\text{B.4b})$$

With the above corrections, we have

$$E_1' - E_0' = E_1 - E_0 + \frac{4C_1 C_2 \cos \theta_+ \sin \theta_-}{E_2 - E_0 - \hbar\omega}, \quad (\text{B.5a})$$

$$E_3' - E_2' = E_3 - E_2 - \frac{4C_1 C_2 \cos \theta_+ \sin \theta_-}{E_2 - E_0 - \hbar\omega}, \quad (\text{B.5b})$$

$$E_2' - E_0' = E_2 - E_0 + \frac{2(C_1 \cos \theta_+ + C_2 \sin \theta_-)^2}{E_2 - E_0 - \hbar\omega}, \quad (\text{B.5c})$$

$$E_3' - E_1' = E_3 - E_1 + \frac{2(C_1 \cos \theta_+ - C_2 \sin \theta_-)^2}{E_2 - E_0 - \hbar\omega}, \quad (\text{B.5d})$$

and

$$\begin{aligned} \langle 1, N |' \hat{H}_0 |0, N+1\rangle' &= -C_1 \sin \theta_+ + C_2 \cos \theta_- \\ &+ (C_1 \sin \theta_+ + C_2 \cos \theta_-) \frac{(C_1 \cos \theta_+)^2 - (C_2 \sin \theta_-)^2}{(E_2 - E_0 - \hbar\omega)^2}, \end{aligned} \quad (\text{B.6a})$$

$$\begin{aligned} \langle 3, N-1 |' \hat{H}_0 |2, N\rangle' &= C_1 \sin \theta_+ + C_2 \cos \theta_- \\ &+ (-C_1 \sin \theta_+ + C_2 \cos \theta_-) \frac{(C_1 \cos \theta_+)^2 - (C_2 \sin \theta_-)^2}{(E_2 - E_0 - \hbar\omega)^2}. \end{aligned} \quad (\text{B.6b})$$

The above equations can now be used to determine the modified conditions for performing the desired operation. One requirement for suppressing the $|0, N+1\rangle \leftrightarrow |1, N\rangle$ oscillations is that the parameters C_1 , C_2 and ω are chosen such that the matrix element $\langle 1, N |' \hat{H}_0 |0, N+1\rangle'$ (equation (B.6a)) vanishes. And in order to obtain full oscillations between the states $|2, N\rangle$ and $|3, N-1\rangle$, the driving frequency ω must match the energy difference $E_3' - E_2'$ (equation (B.5b)). These equations can be solved iteratively starting from the weak-driving relations and calculating corrections. Note however that at some level of accuracy one would need to take into account the coupling between the different blocks in the dressed-state ladder.

It is, however, clear from the above results that strong driving does not simply result in harmless modifications to the required driving frequency and the ratio between the two

driving amplitudes. We identify three processes influencing the performance of the gate. The first effect is related to the energy shifts in the transitions with splittings $E'_2 - E'_0$ and $E'_3 - E'_1$ (equations (B.5c) and (B.5d)). They contain a common shift of $2[(C_1 \cos \theta_+)^2 + (C_2 \sin \theta_-)^2]/(E_2 - E_0 - \hbar\omega)$. This shift represents the ac-Stark shift of the control qubit. For small θ_+ and θ_- , we obtain $2C_1^2/(E_2 - E_0 - \hbar\omega)$, which is the analogue of the ac-Stark shift calculated in section 4.2 (an estimate for this shift using typical experimental parameters is provided there).

Both the control-qubit and target-qubit transitions also get shifted with an amount that is opposite for the two associated transitions: $\pm 4C_1 C_2 \cos \theta_+ \sin \theta_- / (E_2 - E_0 - \hbar\omega)$. What this result means is that during the operation of the CNOT gate, an effective $\hat{\sigma}_z^{(1)} \hat{\sigma}_z^{(2)}$ term appears, which induces a (partial) CPHASE gate, and prevents us from obtaining an ideal CNOT gate. This error is the equivalent of the CPHASE-type error discussed in section 4.2. If we take $J \ll \Delta_1 - \Delta_2$ and the case of strong driving (i.e. $C_1 \sim \Delta_1 - \Delta_2$) we find that the undesirable $\hat{\sigma}_z^{(1)} \hat{\sigma}_z^{(2)}$ term has a coefficient that is of the order of $J^2 / (\Delta_1 - \Delta_2)$, which causes small errors on the timescale of a CNOT gate, which is given by J^{-1} . As discussed earlier, CPHASE-type errors can also be corrected with single-qubit gates.

Lastly, when the matrix elements H_{02} , H_{20} , H_{13} and H_{31} cannot be neglected, it is not possible for any pair of energy levels to be degenerate, which is a general rule of quantum mechanics. As a result no transition can be completely darkened in this case, regardless of the choice of the parameters C_1 , C_2 and ω . To first approximation this source of errors can be regarded as performing an additional single-qubit rotation, which is relatively easy to correct for in experiments.

The results provided in this appendix can be used to perform a detailed numerical study for optimizing the different parameters in order to maximize the fidelity of the CNOT gate in the case of strong driving. However, we shall not do that here.

References

- [1] Geller M R, Pritchett E J, Galiatdinov A and Martinis J M 2010 *Phys. Rev. A* **81** 012320
- [2] Linden N, Barjat H and Freeman R 1998 *Chem. Phys. Lett.* **296** 61
- [3] Plantenberg J H P C, de Groot Harmans C J P M and Mooij J E 2007 *Nature* **447** 836
- [4] Jones J A and Knill E 1999 *J. Magn. Reson.* **141** 322
- [5] Rigetti C, Blais A and Devoret M 2005 *Phys. Rev. Lett.* **94** 240502
- [6] Paraoanu G S 2006 *Phys. Rev. B* **74** 140504
- [7] Makhlin Y, Schön G and Shnirman A 2001 *Rev. Mod. Phys.* **73** 357
- [8] You J Q and Nori F 2005 *Phys. Today* **58** 42
- [9] Wendin G and Shumeiko V 2007 *Low. Temp. Phys.* **33** 724
- [10] Clarke J and Wilhelm F K 2008 *Nature* **453** 1031
- [11] Schoelkopf R J and Girvin S M 2008 *Nature* **451** 664
- [12] Shevchenko S N, Ashhab S and Nori F 2010 *Phys. Rep.* **492** 1
- [13] Ladd T D, Jelezko F, Laflamme R, Nakamura Y, Monroe C and O'Brien J L 2010 *Nature* **464** 45
- [14] You J Q and Nori F 2011 *Nature* **474** 589
- [15] Buluta I, Ashhab S and Nori F 2011 *Rep. Prog. Phys.* **74** 104401
- [16] Averin D V and Bruder C 2003 *Phys. Rev. Lett.* **91** 057003
- [17] Izmailkov A, Grajcar M, Il'ichev E, Wagner T, Meyer H-G, Smirnov A Y, Amin M H S, Maassen A and van den Brink Zagoskin A M 2004 *Phys. Rev. Lett.* **93** 037003

- [18] Plourde B L T, Zhang J, Whaley K B, Wilhelm F K, Robertson T L, Hime T, Linzen S, Reichardt P A, Wu C-E and Clarke J 2004 *Phys. Rev. B* **70** 140501
- [19] Maassen A, van den Brink Berkley A J and Yalowsky M 2005 *New J. Phys.* **7** 230
- [20] Wallquist M, Lantz J, Shumeiko V S and Wendin G 2005 *New J. Phys.* **7** 178
- [21] Bertet P, Harmans C J P M and Mooij J E 2006 *Phys. Rev. B* **73** 064512
- [22] Hime T, Reichardt P A, Plourde B L T, Robertson T L, Wu C-E, Ustinov A V and Clarke J 2006 *Science* **314** 1427
- [23] Hutter C, Shnirman A, Makhlin Y and Schön G 2006 *Europhys. Lett.* **74** 1088
- [24] Niskanen A O, Harrabi K, Yoshihara F, Nakamura Y, Lloyd S and Tsai J S 2007 *Science* **316** 723
- [25] Sillanpää M A, Park J I and Simmonds R W 2007 *Nature* **449** 438
- [26] Yamamoto T, Watanabe M, You J Q, Pashkin Y A, Astafiev O, Nakamura Y, Nori F and Tsai J S 2008 *Phys. Rev. B* **77** 064505
- [27] Helmer F, Mariantoni M, Fowler A G, von Delft J, Solano E and Marquardt F 2009 *Europhys. Lett.* **85** 50007
- [28] Harrabi K, Yoshihara F, Niskanen A O, Nakamura Y and Tsai J S 2009 *Phys. Rev. B* **79** 020507
- [29] Wang Y-D, Kemp A and Semba K 2009 *Phys. Rev. B* **79** 024502
- [30] Strauch F W, Johnson P R, Dragt A J, Lobb C J, Anderson J R and Wellstood F C 2003 *Phys. Rev. Lett.* **91** 167005
- [31] Neeley M *et al* 2010 *Nature* **467** 570
- [32] DiCarlo L, Reed M D, Sun L, Johnson B R, Chow J M, Gambetta J M, Frunzio L, Girvin S M, Devoret M H and Schoelkopf R J 2010 *Nature* **467** 574
- [33] Yamamoto T, Pashkin Y A, Astafiev O, Nakamura Y and Tsai J S 2003 *Nature* **425** 941
- [34] Berkley A J, Xu H, Ramos R C, Gubrud M A, Strauch F W, Johnson P R, Anderson J R, Dragt A J, Lobb C J and Wellstood F C 2003 *Science* **300** 1548
- [35] McDermott R, Simmonds R W, Steffen M, Cooper K B, Cicak K, Osborn K D, Oh S, Pappas D P and Martinis J M 2005 *Science* **307** 1299
- [36] Ashhab S, Matsuo S, Hatakenaka N and Nori F 2006 *Phys. Rev. B* **74** 184504
- [37] Ashhab S and Nori F 2007 *Phys. Rev. B* **76** 132513
- [38] Majer J *et al* 2007 *Nature* **449** 443
- [39] de Groot P C, Lisenfeld J, Schouten R N, Ashhab S, Lupaşcu A, Harmans C J P M and Mooij J E 2010 *Nature Phys.* **6** 763
- [40] Rigetti C and Devoret M 2010 *Phys. Rev. B* **81** 134507
- [41] Chow J M *et al* 2011 *Phys. Rev. Lett.* **107** 080502
- [42] Wei Q, Kais S, Friedrich B and Herschbach D 2011 *J. Chem. Phys.* **135** 154102
- [43] Blais A, Gambetta J, Wallraff A, Schuster D I, Girvin S M, Devoret M H and Schoelkopf R J 2007 *Phys. Rev. A* **75** 032329
- [44] Groszkowski P, Fowler A G, Motzoi F and Wilhelm F K 2011 *Phys. Rev. B* **84** 144516
- [45] Ashhab S, de Groot P C and Nori F 2012 *Phys. Rev. A* **85** 052327
- [46] Beige A, Huelga S F, Knight P L, Plenio M B and Thompson R C 2000 *J. Mod. Opt.* **47** 401
- [47] Filipp S, van Loo A F, Baur M, Steffen L and Wallraff A 2011 *Phys. Rev. A* **84** 061805
- [48] Makhlin Y 2002 *Quantum Inf. Proc.* **1** 243
- [49] Zhang J, Vala J, Sastry S and Whaley K B 2003 *Phys. Rev. A* **67** 042313
- [50] Liu Y-X, Wei L F, Tsai J S and Nori F 2006 *Phys. Rev. Lett.* **96** 067003
- [51] Ferber J and Wilhelm F K 2010 *Nanotechnology* **21** 274015
- [52] Li J, Chalapat K and Paraoanu G S 2008 *Phys. Rev. B* **78** 064503
- [53] Li J and Paraoanu G S 2012 *J. Phys.: Conf. Ser.* **338** 012010
- [54] Gambetta J M, Houck A A and Blais A 2011 *Phys. Rev. Lett.* **106** 030502
- [55] Srinivasan S J, Hoffman A J, Gambetta J M and Houck A A 2011 *Phys. Rev. Lett.* **106** 083601
- [56] Hoffman A J, Srinivasan S J, Gambetta J M and Houck A A 2011 *Phys. Rev. B* **84** 184515

- [57] Nielsen M A and Chuang I L 2000 *Quantum Computation and Quantum Information* (Cambridge: Cambridge University Press)
- [58] Tian L and Lloyd S 2000 *Phys. Rev. A* **62** 050301
- [59] Motzoi F, Gambetta J M, Rebentrost P and Wilhelm F K 2009 *Phys. Rev. Lett.* **103** 110501
- [60] Galiatdinov A, Korotkov A N and Martinis J M 2011 arXiv:1105.3997
- [61] Ashhab S, Niskanen A O, Harrabi K, Nakamura Y, Picot T, de Groot P C, Harmans C J P M, Mooij J E and Nori F 2008 *Phys. Rev. B* **77** 014510